

## TABLE OF CONTENTS

	<u>Page</u>	
I. SUMMARY	1	1/A5
II. INTRODUCTION	3	1/A7
III. COMPOSITE CONDUCTOR PROPERTIES	7	1/A11
IV. EXPERIMENTAL EQUIPMENT AND SPECIMENS	19	1/B9
V. RESULTS AND DISCUSSION	37	1/C13
A. THERMAL DATA OF INDIVIDUAL SPECIMENS	38	1/C14
1. THERMAL CONDUCTIVITY RESULTS	38	1/C14
2. PEAK HEAT FLUX DENSITIES	45	1/D7
3. INFLUENCE OF ADDITIONAL INSULATING COATINGS	58	1/E6
4. QUENCH ONSET DATA	63	1/E11
5. HEAT TRANSFER COEFFICIENTS	66	1/E14
B. HEAT CAPACITIES	72	1/F6
C. CONDUCTOR ASSEMBLY RESULTS	74	1/F8
D. FRICTION RESULTS	80	1/F14
VI. CONCLUSIONS	83	1/G3

APR 25 1978

Don 880-1-14

NAS 1.26: 2963

NASA Contractor Report 2963

COMPLETED  
ORIGINAL

# Cryogenic-Coolant He<sup>4</sup>-Superconductor Interaction

S. Caspi, J. Y. Lee, Y. I. Kim,  
R. J. Allen, and T. H. K. Frederking

GRANT NSG-3153  
APRIL 1978

**NASA**

**NASA Contractor Report 2963**

# **Cryogenic-Coolant He<sup>4</sup>-Superconductor Interaction**

**S. Caspi, J. Y. Lee, Y. I. Kim,  
R. J. Allen, and T. H. K. Frederking**  
*University of California at Los Angeles  
Los Angeles, California*

**Prepared for  
Lewis Research Center  
under Grant NSG-3153**

**NASA**  
National Aeronautics  
and Space Administration

**Scientific and Technical  
Information Office**

**1978**

BLANK PAGE



## I. SUMMARY

The main impact of the present investigations has been in the area of post-quench behavior of composite (type II - normal metal) superconductors. A special superconductor with an approximate square cross section (with edges rounded off) permitted installation of central heaters and thermometers inside the composite. The heater simulation employed covered various thermodynamic regimes of He<sup>4</sup>. They included near-saturated liquid, He II at low pressures and at pressures above the thermodynamic critical value, and pressurized He I. Overall thermal conductances were evaluated from the runs at quench onset conditions. These and other data substantiate improvements based on the use of liquid He II which have been reported elsewhere for non-superconducting heater simulation tests.

The findings show an attractiveness of He II from the post-quench protection point of view. Thus, smaller stabilizer thicknesses are an immediate result of these studies. This improvement may not be very significant when thick formvar layers are employed. The latter are needed not only from the thermal point of view but also for dielectric reasons. The present data show that any composite with electrical insulation may be operated in one or another safety regime. When thick formvar coatings are employed it is the transition temperature of the superconductor which will govern the quench onset of the heater simulation technique. On the other hand when very thin coatings are employed, the surface heat flux density may be the decisive post quench factor. As the thermodynamic state of the fluid was varied, safety conditions did change from one regime to another. In other words, the existing insulator layer may be "thin" in one case, and "thick" in another thermodynamic state of the fluid. From the present quasi-steady simulation point of view, an optimum appears to be an approach which satisfies both criteria at the same time by choosing the limiting thickness (or its vicinity respectively). In these deliberations for the safety design, the effect of transients are not included.

A few data were obtained in the area of friction forces during relative conductor motion. The friction coefficients obtained in the present runs

indicate that some attention has to be paid to the preservation of a well-defined winding package geometry. Otherwise the magnitude of the friction factor has the potential of causing local quenches during relative conductor motion.

## II. INTRODUCTION

Superconductivity has been utilized in novel energy and transportation equipment. Efforts toward large system development have included conceptual design and prototype testing. Usually several constraints are imposed which may vary from one type of equipment to another. For instance, extreme safety precautions have been demanded for fusion energy magnet systems. The latter incorporate full cryostatic stabilization of composite superconductors (mostly NbTi-Cu). In other systems these stability measures however, are in conflict with requirements of high energy densities (energy per unit mass). Examples are mobility and flight systems including electromechanical energy converters. To satisfy demands for compact equipment, wire manufacturers have marketed composites for large magnets which use considerably less normal metal stabilizer mass than other more conservative designs.

In recent R & D work the Plasma Physics Branch of the Lewis Research Center of the National Aeronautics and Space Administration (NASA) has completed a conceptual design of a  $\frac{1}{2}$ -meter active-channel-length MHD superconducting magnet. Formvar-insulated superconducting wire (composite of copper and Nb-48-Ti) has been purchased by NASA for this project. However inadequate thermal property results and low temperature frictional data exist for this type of conductor. It is significant for the final engineering design to eliminate property uncertainties. Therefore, thermal and frictional investigations have been conducted at the Cryo-Lab (University of California, Los Angeles) during the last three months.

The designer's data needs are not restricted to thermophysical properties alone. Usually at least two phase transitions may accompany operational anomalies: First, the transition from the superconducting state to the normal state (quench); second, fluid phase transitions (e.g. liquid to vapor, He II to He I). It is mandatory to safeguard against undesirable consequences of both phase transitions during a severe quench. Related design measures have become known as "stability" criteria. In principle the two different kinds of phase transitions are characterized by sets of independent parameters. Some quantities governing quench conditions are the transition temperatures (which depend on the magnetic field), the concentration of Nb and other constituents, and the metallurgical treatment. The set of parameters governing a fluid phase

transition includes quantities such as fluid transport properties and thermodynamic equilibrium conditions. Further, "thermal switching" can occur when one fluid phase is replaced by another one. This in turn may cause temperature excursions. Thermal switching is a consequence of a negative slope of the function which describes the heat flux density  $q$  versus the temperature difference  $\Delta T$  between the solid and the bulk fluid temperature. It is this boundary condition which represents an important link with the solid system. As the solid power generation is controlled by external circuit impedance and normal metal parameters, system operation may be unstable for some post-quench scenarios in a certain range of  $\Delta T$ . Accordingly, a complex interaction between solid system and surrounding cryo-coolant may result.

Very little information appears to be available about this interaction when friction takes place during relative motion of adjacent conductor sections. More information appears to be known for special quantities of some conductors (e.g. propagation velocity of the quenched-domain phase boundary; steady heat transfer from a normal metal). Relatively little appears to be documented in particular about two effects: First, the influence of the formvar coating; second, the effect of variations of the thermodynamic state of the coolant. Our studies have dealt with several quantities related to both problem areas.

To gain a meaningful perspective of the impact of the post-quench information on system design we list briefly an example (Table II.1 for conventional cooling by saturated liquid He<sup>4</sup> near its normal boiling point ( $T = 4.2$  K)). Relevant quantities for the present thermal studies are items 2 and 3 in Table II.1. The choice of the normal metal mass, and the selection of the formvar thickness. Historically, criterion 3 (Table II.1) has been an important point of the early stabilization approach published by Stekly and Kantrowitz (References 1 and 2). Subsequently, however Boom, et al. (Reference 3) demonstrated on the basis of heater simulation techniques that the limiting heat flux density of liquid He I (item 2) may be of even greater concern provided no significant metal insulator coatings are applied. Accordingly, the designer may select certain elements or combinations of various components for optimization of safety conditions. It should be kept in mind that there is no complete safety as assured by the design procedures outlined in Table II.1. Drastic anomalies may invalidate any safety design. Examples are the loss of magnet coolant, overpressurization, pressure reduction due to expulsion of cryo-fluid

TABLE II.1

SIMPLIFIED CRITERIA FOR THE SAFETY DESIGN ILLUSTRATED FOR NEAR-SATURATED  
He I AT NBP ( = 4.2 K )

	COMPONENT	DESIGN QUANTITY	BASIC CRITERION	CONSEQUENCE OF ANOMALOUS OPERATION e.g. OVERLOAD )
1	TYPE II FILAMENT	DIAMETER	FLUX JUMP SUPPRESSION VALUE (CRITICAL DIAMETER )	DISSIPATION FROM FLUX JUMPS
2	NORMAL METAL STABILIZER	THICKNESS OR MASS	LIMITING HEAT FLUX DENSITY AT SURFACE WETTED BY FLUID	NUCLEATE BOILING REPLACED BY FILM BOILING; TEMPERATURE EXCURSION; FLUID DENSITY REDUCTION; DIELECTRIC BREAKDOWN
3	INSULATING COATING	THICKNESS	TRANSITION TEMPERATURE $T_{80}$ FROM SUPERCONDUCTING TO NORMAL STATE	PHASE TRANSITION TO NORMAL STATE; DISSIPATION (JOULE HEATING); PROPAGATION OF NORMAL DOMAIN

into vacuum spaces and others. Aside from these rather extreme cases however, it appears to be justifiable to search for improved thermodynamic states of the cryo-coolant. Examples are utilization of superfluidity effects, subcooled boiling at near-critical pressures ( $P \approx P_c$ ), and supercritical pressures ( $P > P_c$ ).

Therefore, the present studies had the specific purpose of determining suitable thermodynamic states by measuring thermal boundary conditions of the formvar-coated conductor. A heater simulation technique was used in various regions of cryo-fluid He<sup>4</sup> including temperatures below the lambda curve ( $T < T_\lambda$ ), and  $P \geq P_c$ . In the evaluation of records emphasis has been placed on extraction of information from the experimental records which is crucial for safety in a post-quench scenario. Examples are the take-off heat flux densities and the  $q$  values at the onset of normal domain formation. The entire range of possible post-quench scenarios contains many subsets. As a first step toward the goal of obtaining a comprehensive design data basis, the solid-cryocoolant interaction during quasi-steady transport has been of concern in the present studies of the Cu-NbTi composite superconductor.

### III. COMPOSITE CONDUCTOR PROPERTIES

Prior to the thermal and friction experiments several properties of the solid composite have been determined. In addition, surface and interface conditions at the normal metal-type II filament boundary have been inspected.

Boundaries and Geometry. Figure III.1 is a cross sectional picture of the present composite. There are 48 type II filaments of Nb-48-Ti alloy. These filaments do not show a uniform perfectly circular cross section. The deformations appear to be unavoidable byproducts of the manufacturing process. Similarly, the outer boundaries of the composite do not show a perfect square shape and the edges are rounded off.

The type II-normal metal transition layer as recorded by electron microprobe is shown in Figure III.2. X-ray back scattering indicated a rough interface, possibly with surface asperities of several  $\mu\text{m}$  height. The electron beam has a width of about 1 to 2  $\mu\text{m}$ . Accordingly, the transition layer of Figure III.2 is quite comparable to the beam width. No excessive interface resistance should be expected under these conditions provided the temperature is not very low ( $T > 2\text{K}$ ).

The formvar surface at the outer conductor boundary appears to be relatively shiny. This indicates that the asperities of the micro-geometry are not larger than the wave length of light. The macro-shape was assessed using a surface profilometer (radius of stylus tip 0.050 cm). Examples of the recorded profiles perpendicular to the conductor axis are shown in Figures III.3a and b. Surface variations recorded were in the range from about 5  $\mu\text{m}$  to about 30  $\mu\text{m}$ .

The distance from one surface to another (nearly parallel) surface was determined from a number of micrometer measurements. From several data sets the following averages were obtained:  $0.2237 \pm 0.0003$  cm,  $0.2226 \pm 0.0002$  cm, and  $0.2212 \pm 0.0002$  cm. The other set of readings (averages) for the surface pair perpendicular to the first one were obtained as follows:  $0.2252 \pm 0.0003$  cm,  $0.2249 \pm 0.0004$  cm,  $0.2241 \pm 0.0001$  cm. Accordingly, there are systematic departures from the square cross section. Taking the

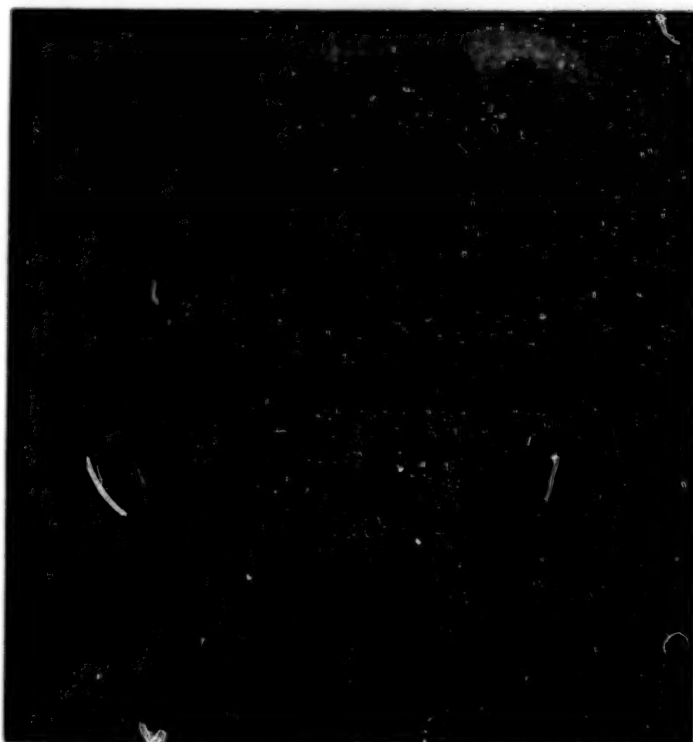


**Figure III.1. Cross sectional picture of composite conductor**



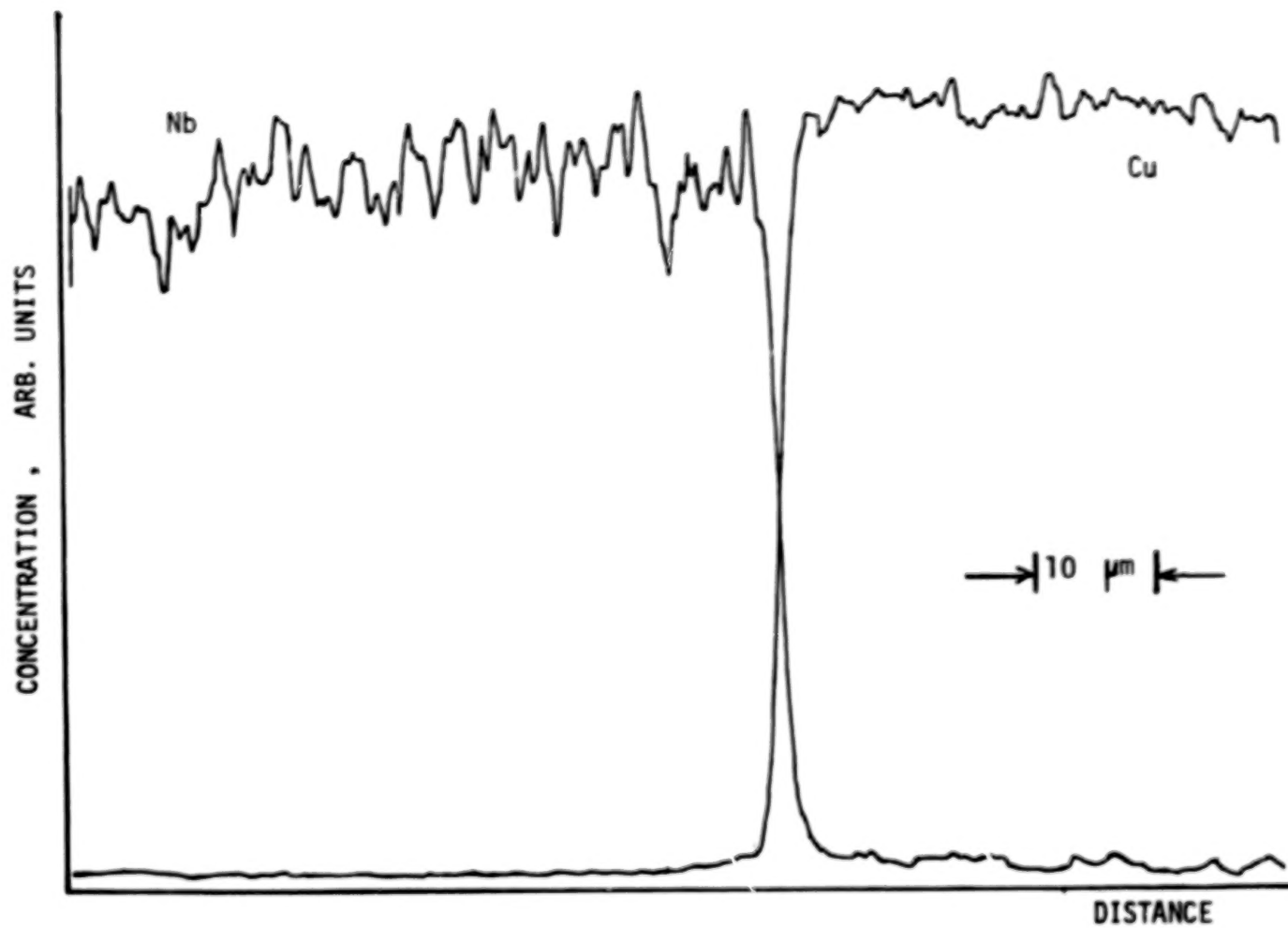
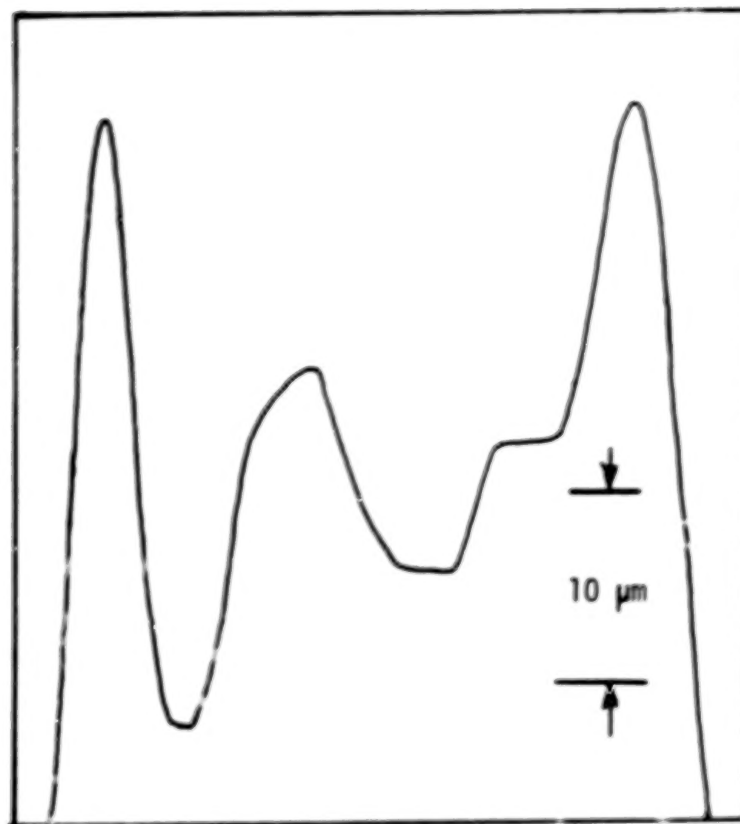
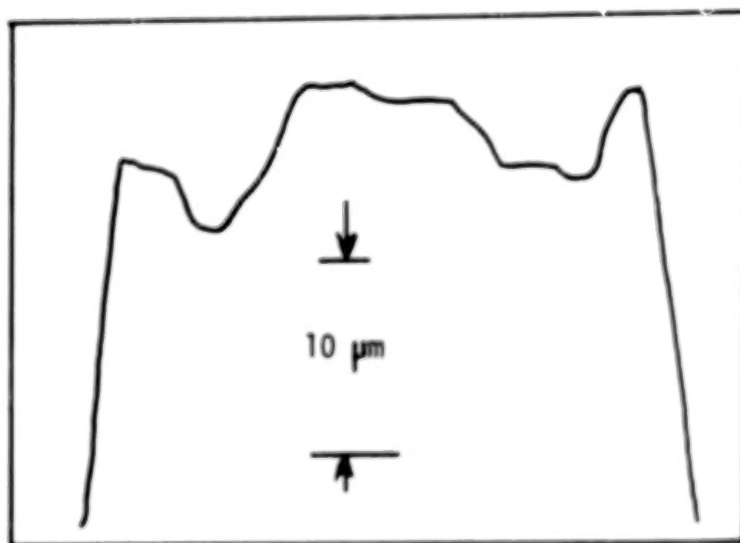


Figure III.2 . Electronmicroprobe record of transition layer between type II and Cu



(a)



(b)

Figure III.3. Surface profilometer records of formvar-coated composite in transverse direction; (a) Side I; (b) Side II

average of these numbers we obtain a conductor thickness (including the formvar layer) of  $0.2236 \pm 0.0019$  cm. The formvar layer thickness was also not constant. The local conditions inspected are characterized by the following values: First surface pair of nearly parallel planes:  $23.5 \pm 1.0$   $\mu\text{m}$ , second surface pair:  $40.2 \pm 3.1$   $\mu\text{m}$ . The mean value of the thickness obtained from these data is  $31.8 \pm 4.1$   $\mu\text{m}$ . In the subsequent data reduction a thickness of  $d_{\text{FV}} = 30$   $\mu\text{m}$  has been used. This procedure appears to be justifiable as there are uncertainties related to the rounded edges and other conditions (e.g. macro-shape variations of the surface profilometer tests).

The entire solid cross section including formvar insulation was determined at one location as  $4.80 \pm 0.11$  (i.e.  $\pm 3\%$ )  $\text{mm}^2$ . The circumference (including formvar) turned out to be 8.1 mm. (The thermal conductivity of the formvar was evaluated from the power runs described subsequently).

Normal Metal Stabilizer. In the T-range from the transition temperature  $T_{\text{sn}}$  to 300 K, the normal metal has an electrical resistance quite close to  $R$  of the composite ( $\leq 1\%$  difference). This is a consequence of the rather large electrical resistance of the type II alloy in the normal state. Some properties of this alloy have been obtained from thermal investigations with instrumented specimens (described subsequently). In addition, two samples were mounted in the vapor above a 4.2 K bath. Specimen C-01 (short helix of about two turns with axis positioned vertically) had formvar insulation. Specimen C-02 cut from uninsulated wire was rather short (length 2.68 cm).

The residual resistivity ratio (RRR) of the copper of specimen C-01 was  $\text{RRR} = R_{295}/R_{T_{\text{sn}}} = 150$ . This value appears to be affected slightly by deformation of the wire to the helix winding diameter of about 6.8 cm. Specimen C-02, on the other hand, had a value of  $\text{RRR} = R_{294}/R_{T_{\text{sn}}} = 173$ .

The thermal conductivity  $k(T)$  of the copper in longitudinal direction was calculated from the Lorenz number of free electrons ( $L_e = 2.45 \cdot 10^{-8} \text{ W K}^{-2} \Omega$ )

$$k = (RRR) T (L_e / \rho_T) \quad (\text{III.1})$$

( $\rho_T$  = electrical resistivity at temperature T; e.g.  $\rho_{295}$  for T = 295 K). An electrical resistivity of  $\rho_{295} = 1.68 \mu\Omega \text{ cm}$  was used from Reference 49. This value agrees reasonably with the data for Cu listed by Brechna (Reference 50). In general the composite specimens show a higher resistivity. The present data for  $\rho_{295}$  and Brechna's values (related to T = 295 K) for technology materials were a few % above corresponding data for very pure copper.

At T = 1 K the resulting thermal conductivity-values are: C-01:  $2.19 \text{ W cm}^{-1} \text{ K}^{-1}$ ; C-02:  $2.52 \text{ W cm}^{-1} \text{ K}^{-1}$ . At 4.2 K the thermal conductivities are  $9.2 \text{ W cm}^{-1} \text{ K}^{-1}$  (C-01) and  $10.6 \text{ W cm}^{-1} \text{ K}^{-1}$  (C-02). Stekly (Reference 48) lists  $7.0 \text{ W cm}^{-1} \text{ K}^{-1}$ .

The thermal conductivities discussed so far are longitudinal k-values. However, k of NbTi-composite is anisotropic (Reference 4). As the type II filaments of low k-values occupy a fraction of the volume, they impede the radial flow of heat more than the longitudinal transport. Figure III.4 plots the present results along with data of Reference 4 for sections of a coil (Cu-NbTi composites). Further, an additional OFHC-value is included in Figure III.4. This result has been deduced from the residual resistance ratio  $R_{295}/R_{4.2} = 44.4$  for a Cu-tube (O.D. 0.635 cm, I.D. 0.317<sub>5</sub> cm) which was deformed considerably by bending it to a winding diameter of about 4 cm; (at T = 1K:  $k = 0.647 \text{ W cm}^{-1} \text{ K}^{-1}$ ).

Two methods were employed to determine the Cu-cross section. One approach was the weight determination of the uninsulated composite prior to and after removal of Cu (by etching). The formvar layer had been stripped away before weighing. The resulting Cu-cross section was  $A_{\text{Cu}} = 0.0312 \pm 0.0005$  (i.e.  $\pm 4\%$ )  $\text{cm}^2$ .

The other method was based on the optical determination (Fig. III.1) of the total filament cross section. The results are discussed below.

Type II Filament. Aside from the optical inspection, further details of the filament geometry were obtained by the removal of the Cu. In addition, the transition temperature  $T_{\text{sn}}$  and the electrical resistivity were determined.

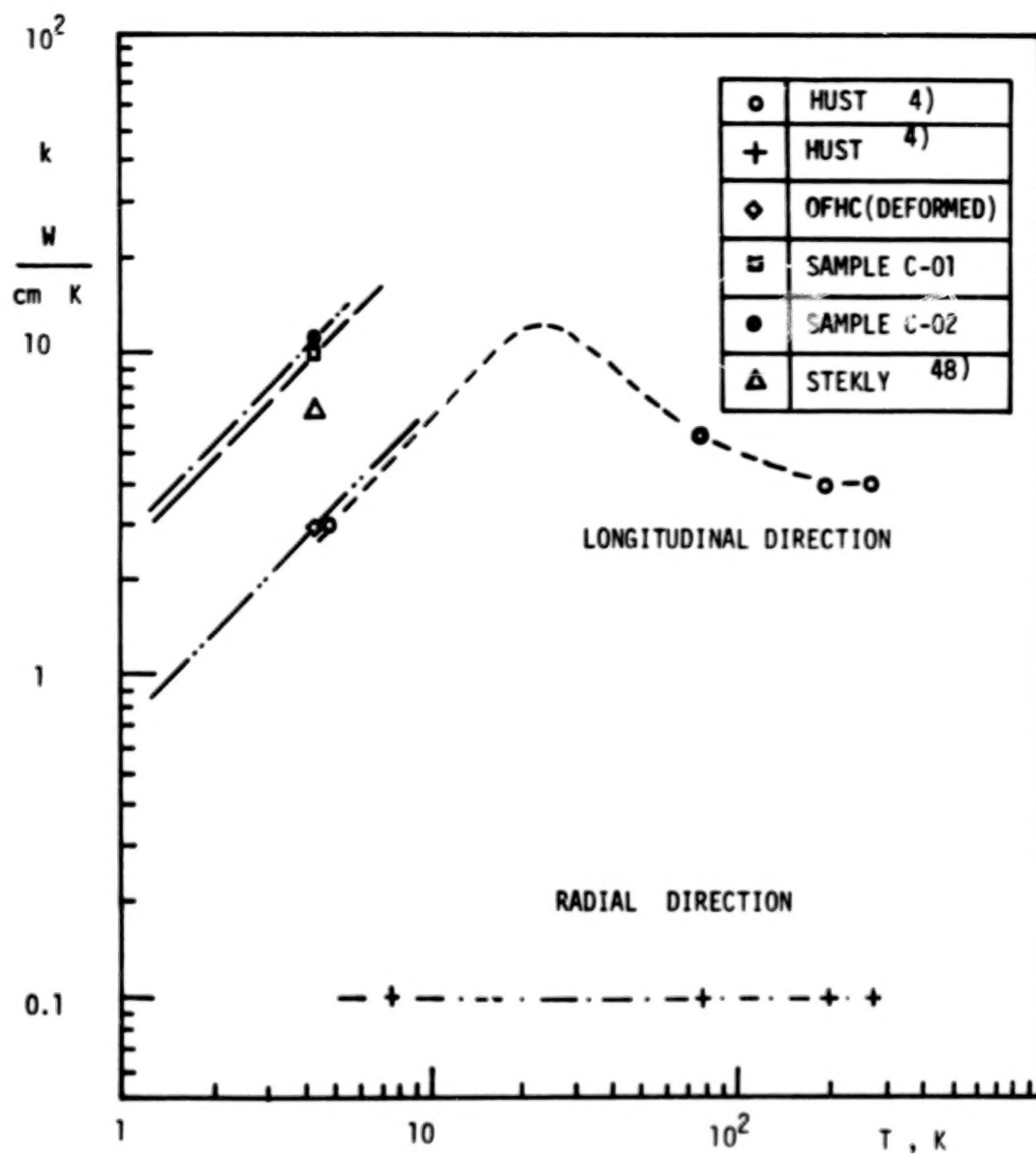


Figure III.4 . Thermal conductivity of Cu-stabilizer

The transition temperature of the type II superconductor was evaluated from two different types of measurements. One method made use of a vapor environment above a 4.2 K bath (specimen IS-3B of the subsequent section). The transition temperature  $T_{sn} = 8.9 \pm .2$  K was obtained. The second approach utilized the onset of normal resistance during power runs. From 29 records  $T_{sn} = 8.56 \pm 0.22$  K resulted; (extreme limits of these runs were 8.2 K and 9.0 K). These values appear to be quite consistent with the data of Reference 5.

In the literature (References 5 to 7) transition temperatures above and below  $T_{sn}$  of pure Nb have been reported. The details depend on impurities, alloying and heat treatment of the Nb-Ti alloy. For the present Nb-48-Ti material it appears to be possible that the metal adjacent to the filament boundary may have a transition temperature which departs from the bulk filament value.

Electrical resistivity data are shown in Figure III.5 versus  $T$  for the normal state of type II superconductors as  $\rho_{el}(T)$ . Data from References 6,7,11 are included in this plot. The electrical resistivities at  $T_{sn}$  in the normal state appear to be consistent with Reference 8. Further, we note that the thermal conductivity of Nb-48-Ti has been measured by Y.W.Chang (Reference 9). The latter Reference (Part III) compares the  $k$ -data obtained with other literature results for Nb-Ti alloy. (Additional Nb-Ti properties have been discussed in Reference 10).

The weight determination gave a mean filament diameter of  $\bar{D}_F = 176 \mu\text{m}$ . This  $\bar{D}_F$ -value was deduced by measuring the lengths of the entire set of 48 filaments. Results of optical measurements are discussed in Figure III.6. As the filament cross sections were not perfect circles, an equivalent diameter was found for each cross section. Figure III.6 plots the filament diameter distribution function  $(\Delta N_F / \Delta D_F)$ . Mean diameters of  $\bar{D}_F = 185 \mu\text{m}$  and  $180 \mu\text{m}$  were found.

Cryostatic Safety Measure. A frequently used approach toward cryostatic sizing of the Cu-stabilizer is based upon steady state postquench conditions (Reference 3) in conjunction with several assumptions, e.g. initiation of a local quench at one single nucleus. Further, a useful reference quantity has been the heat flux density of recovery ( $q_R$ ) for a

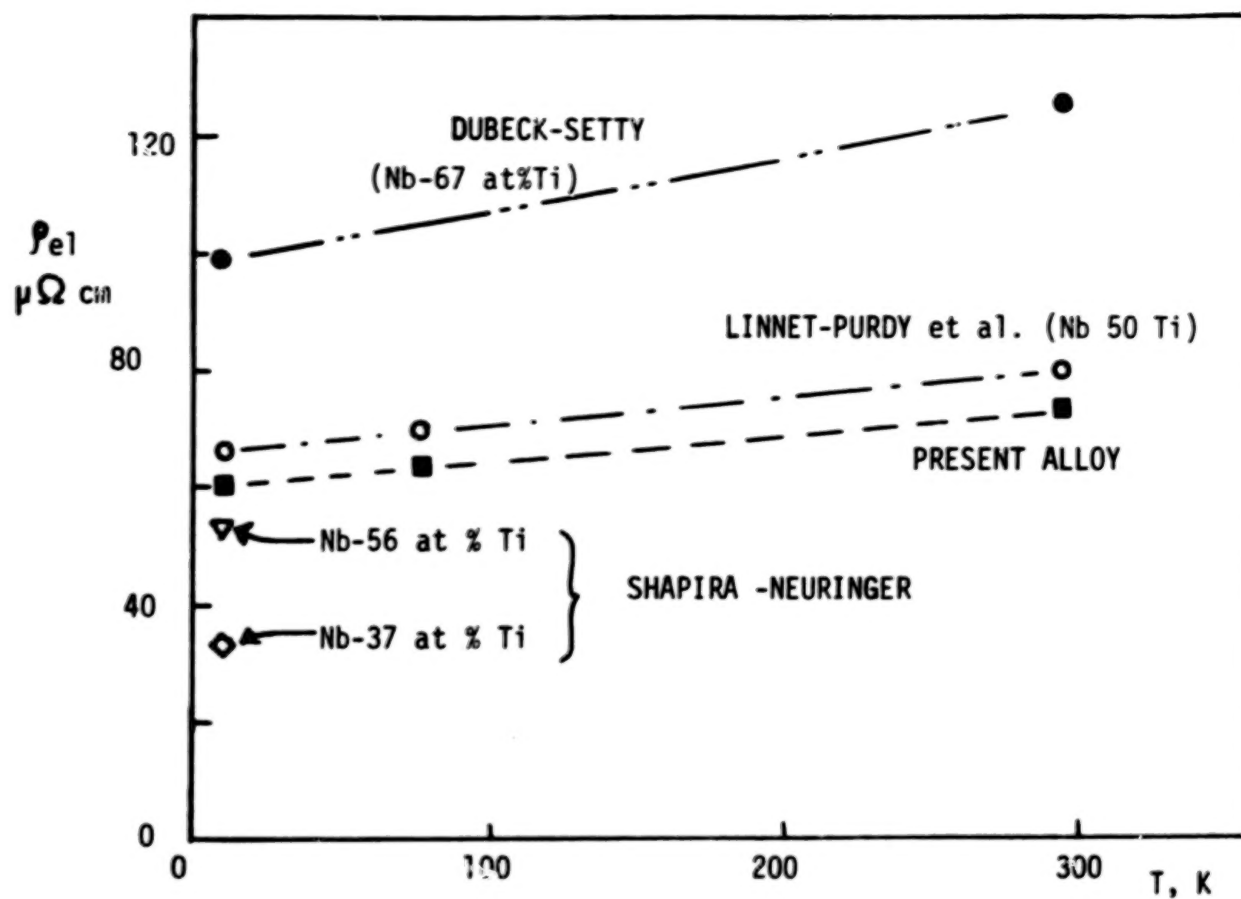


Figure III.5 . Electrical resistivity of Nb-Ti alloys in the normal state

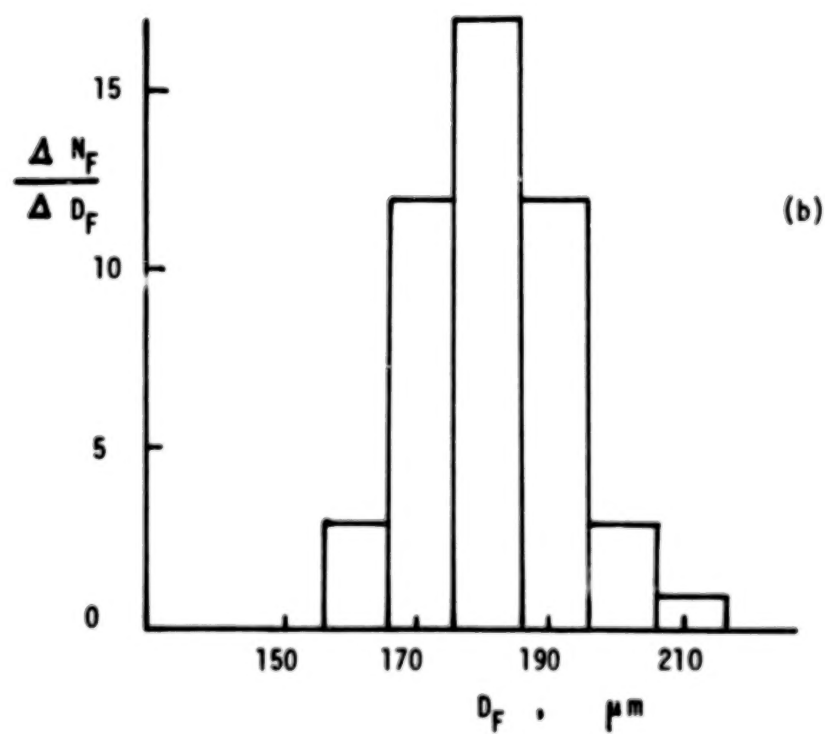
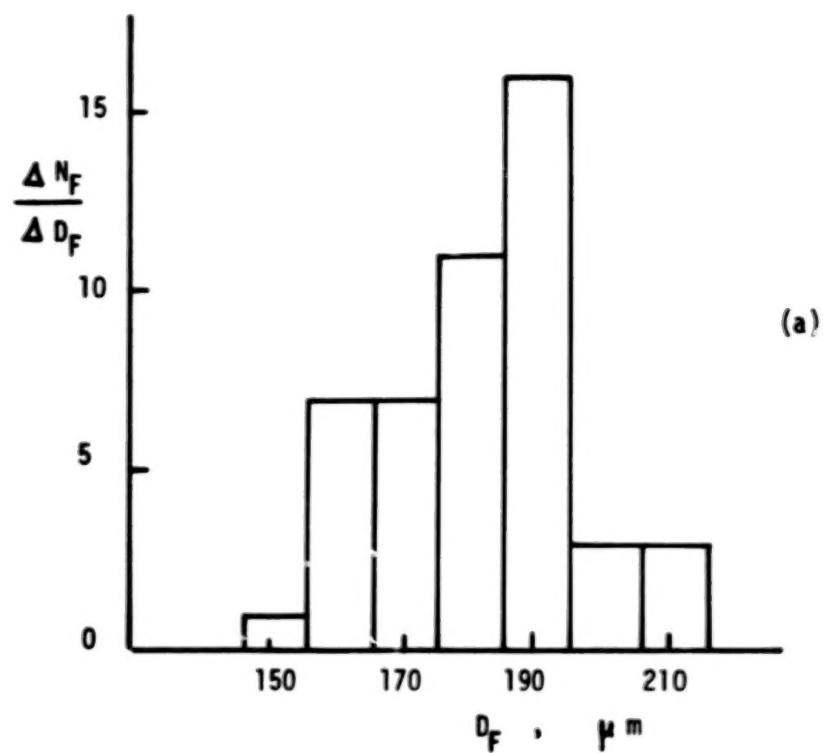


Figure III.6 . Filament diameter distribution;  
(Two data sets a , b )



horizontal conductor geometry. The value considered by some authors for He I at 4.2 K is  $0.4 \text{ W/cm}^2$ . After insertion of  $q_R$  into the steady state stability condition  $I^2 \rho_{cu} / A_{cu} = q_R C_c$  we may express the Cu to type II cross sectional ratio (where  $A_{tot} = A_{cu} + A_{II}$ ) in the following equation as required quantity (subscript Req)

$$\left\{ \frac{A_{cu}}{A_{II}} \right\}_{Req} = \frac{1}{(q_R C_c A_{tot} / \rho_{cu} I^2) - 1} \quad (III.2)$$

( $I$  = design transport current,  $C_c$  = circumference wetted by the cryo-coolant,  $\rho_{cu}$  = electrical resistivity of the copper at  $T_{sn}$  when the conductor is in the normal state). Meaningful solutions to Equation (III.2) require a denominator different than zero. The limiting current resulting from a vanishing denominator is designated as  $I_L$ . For the present geometry and  $RRR = 160$  we obtain  $I_L \approx 1.2 \cdot 10^3 \text{ A}$ .

For further illustration of the safety condition we select a design value of  $I = 830 \text{ A}$ . For this choice Eq. (III.2) predicts a required cross sectional area ratio (for  $q_R = 0.4 \text{ W/cm}^2$ ) of  $(A_{cu}/A_{II})_{Req} = 0.87$ .

From the previous determination of the total cross sectional area and the mean filament diameter ( $\bar{D}_F \approx 180 \mu\text{m}$ ) we obtain a Cu-cross sectional area  $A_{cu}$ . After subtraction of the formvar cross sectional area we have  $(A_{cu} + A_{II}) = 0.0456 \text{ cm}^2$ . The resulting ratio is  $(A_{cu}/A_{II}) = 2.74$ .

A related safety measure is useful for a quantification of the stabilization achieved. We introduce a "cryostatic safety factor"

$$F_{cs} = \frac{A_{cu}/A_{II}}{(A_{cu}/A_{II})_{Req}} \quad (III.3)$$

For the present set of data (He I at 4.2 K) we obtain  $F_{cs} \approx 3.1$ . Therefore, the present composite conductor appears to have been designed conservatively, from the point of view of the cryostatic safety/stability concept. This condition however refers only to one particular thermodynamic choice of the state of the coolant.

Table III.1 is a list of essential dimensions of the composite discussed in this Section III.

TABLE III . 1

## COMPOSITE PARAMETERS (Nb-Ti-Cu-FORMVAR)

Total cross section of the composite	$A_{tot} , \text{cm}^2$	$4.80 \times 10^{-2}$
Circumference of the composite	$C_c , \text{cm}^2/\text{cm}$	0.81
Cu-cross section	$A_{cu} , \text{cm}^2$	0.033
Insulator (formvar) Thickness	$d_{FV} , \mu\text{m}$	30
Type II filament diameter	$\bar{D}_F , \text{cm}$	0.018
Conductor thickness	$a , \text{cm}$	0.224
Radius of curvature at conductor edges	$R_c , \text{cm}$	0.05
Transition temperature at inner surface	$T_{sn} , \text{K}$	8.56
Transition temperature of filament	$T_{sn} , \text{K}$	8.9

$$\text{IDEAL CIRCUMFERENCE: } C_c = 4a + 2\pi R_c - 8 R_c$$

$$\text{IDEAL TOTAL CROSS SECTION: } A_{tot} = a^2 - R_c^2(4 - \pi)$$

#### IV . EXPERIMENTAL EQUIPMENT AND SPECIMENS

Equipment In most of the present experiments use has been made of an existing cryostat system. It provided facilities and related instruments to obtain a saturated liquid He<sup>4</sup> bath from 4.2 K to He II temperatures. For studies with pressurized cryofluid He<sup>4</sup> an additional system of various components was inserted into the cryostat and connected to an external pressurization system. Figure IV .1 is a schematic of the assembly.

A pressure reservoir was provided by a compressed He<sup>4</sup> gas cylinder at room temperature. A regulator permitted selection of a constant pressure suitable for the low temperature work. The pressurized gas was cooled down by a set of heat exchangers inserted into the cryostat. After temperature reduction of the He gas, the pressurized test chamber permitted good thermal contact with the outer liquid He<sup>4</sup> bath. The overall system was built with a downstream exhaust section in order to provide facilities for finite flow experiments (if so desired).

A first stage of the heat exchanger coils was a helix exchanger (Cu O.D. .476 cm {3/16 in}) immersed in liquid nitrogen . The pressurized He<sup>4</sup> leaving the N<sub>2</sub> exchanger had a temperature of about 80 K. In the He<sup>4</sup> cryostat a set of spirally wound exchanger sections were cooled by vapor escaping from the liquid He bath. The two exchanger systems were connected by a transfer tube made of stainless steel. It consisted of two concentric tubes forming an annulus. This annulus was evacuated during the runs.

The interior spirals were also made out of copper (O.D. .476 cm {3/16 in}). The entire systems had 11 sets of spirals with five turns each. Leaving this exchanger system at about 6 K (according to design calculations), the pressurized He<sup>4</sup> entered a third stage heat exchanger located in the cryostat pool. The size of the tubing in this subsystem was reduced to an O.D. of .316 cm (1/8 in). There were three spirals with six turns in each set. This final stage equilibrated the pressurized He with the outer bath temperature prior to entry into the test chamber.

The test section size was selected to accommodate mounting in the pressure chamber. The chamber was made out of brass and consisted of a cylindrical can (O.D. 5.65 cm ) and a top flange carrying 12 screws. Sealing of the chamber was accomplished with a home-made indium O-ring.

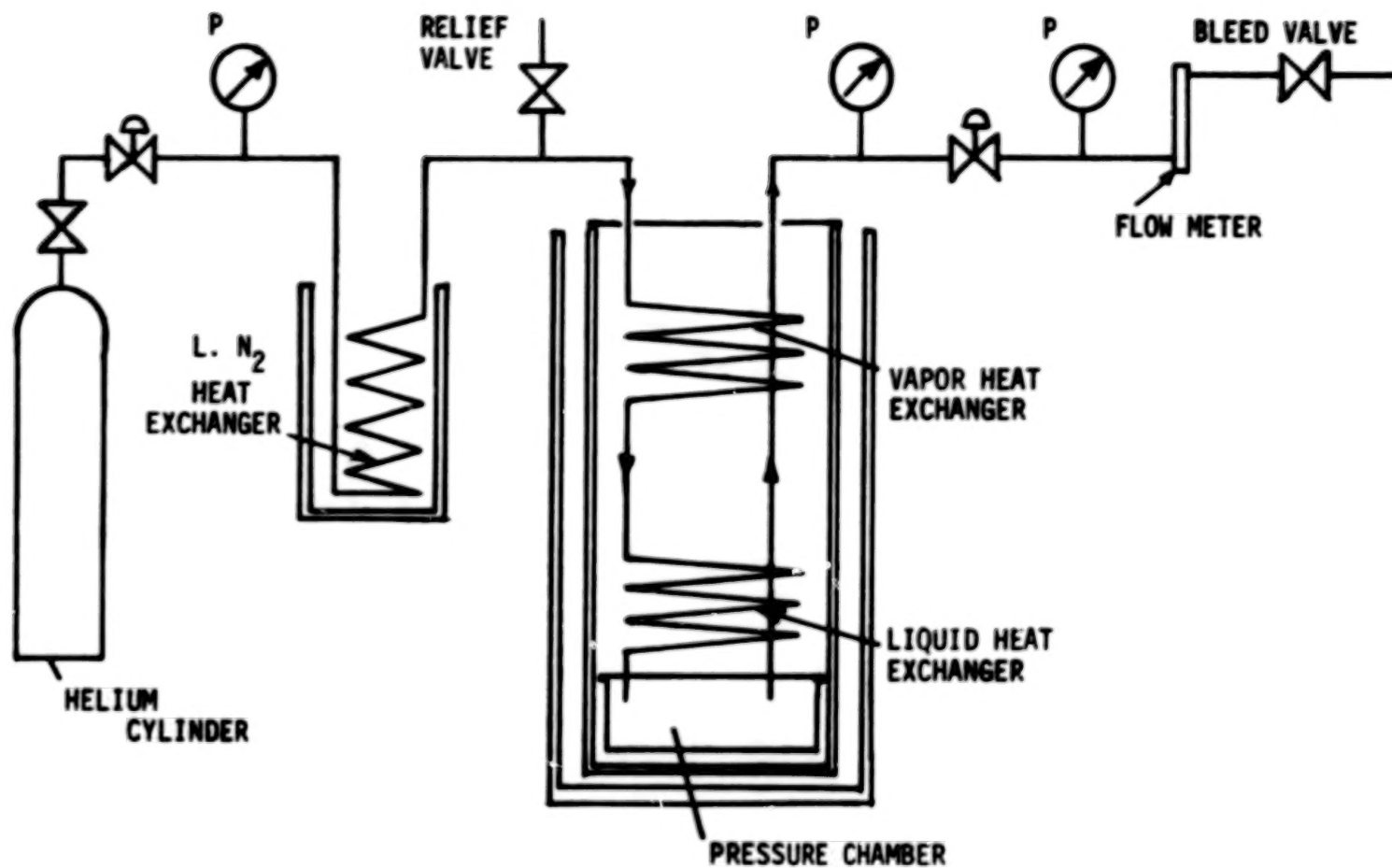


Figure IV.1 . Schematic of cryosystem

Specimens. Various samples cut from the composite conductor have been instrumented for thermometry and equipped with constantan heaters mounted in central axial holes. First a drill with a diameter of 0.117 cm ( 46 mil O.D.) was selected for the machining of holes. This choice had the purpose of minimizing damage to the type II filaments. This diameter could be handled safely for hole lengths up to about 1.25 cm ( $\frac{1}{2}$  in.) without causing significant problems related to the presence of the soft copper. The specimens of a total length of 2.54 cm ( 1 in.) were manufactured by drilling holes from both ends. A schematic of a composite specimen (designation : IS- 2 ) is shown in Figure IV. 2 . Major properties of various specimens are summarized in Table IV.1

Figure IV. 2 is a cross section through the axis of the specimen. A central carbon thermometer ( Allen-Bradley-Ohmite, nominal room temperature resistance 39 Ohm) measured the temperature at the inner surface of the composite conductor. A stainless steel tube (hypodermic needle size of .0559 cm O.D. ) served as heater support . The constantan heater wire had a diameter of about 0.0075 cm and was teflon-insulated. There were two heater sections on each side of the thermometer , as indicated in Figure IV.2 . The sealing method used was similar to the procedure of Goodling and Irey (Reference 12 ) . These latter authors have noted that considerable care is needed for epoxy-sealed ends . For sample IS-1 epibond was used satisfactorily. It is noted though that failures are always possible , as pointed out in the literature (Reference 13 ) .

Table IV.1 lists modified additional composite samples . Modification IS-1S had two current leads to the copper-type II-composite and potential taps for resistance thermometry . The leads for the measuring current consisted of another multifilament superconducting wire (Nb11 alloy, diameter 0.040 cm) . The potential taps had constantan wire section at the specimen to minimize heat leaks. At the end of various runs with specimen IS-1 S the formvar insulation was removed

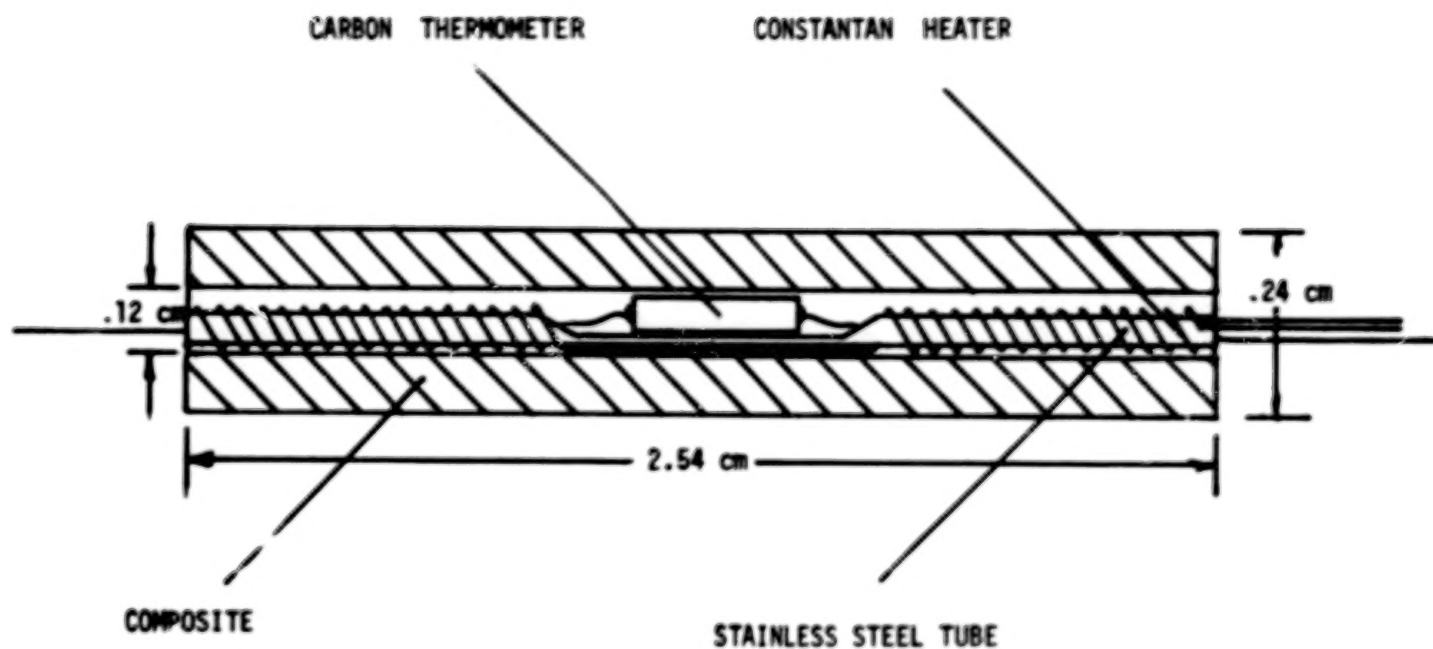


Figure IV. 2. Cross section of specimen (used in sample DS-2 )

TABLE IV .1

## SPECIMENS

DESIGNATION	POSITION	LENGTH OF TEST SECTION	REMARKS
IS-1	AXIS : HORIZONTAL; "DIAMOND" CROSS SECTION	2.17 cm	WETTED AREA: 1.74 <sub>9</sub> cm <sup>2</sup>
IS-1S	SAME AS	IS-1	COMPOSITE INSTRUMENTED AS RESISTANCE THERMOMETER
IS-1B	SAME AS	IS-1	FORMVAR REMOVED; AREA : 1.73 cm <sup>2</sup>
IS-2	AXIS : HORIZONTAL; CROSS SECTION	2.40 cm	MOUNTED IN PHENOLIC; TOP AREA WETTED: 0.483 <sub>6</sub> cm <sup>2</sup>
IS-3A/B	AXIS : HORIZONTAL; "DIAMOND"	1.95 cm	VACUUM INSULATION; 1.71 cm <sup>2</sup> A: Pt-10 % Rh; B: CONSTANTAN HEATER
DS-1A	AXIS : HORIZ. "DIAMOND"	2.17 cm	DUAL-SPECIMEN; TOP WIRE WITH THERMO- METER;
DS-1B	SAME AS DS-1A	2.17 cm	G-10 SPACER INSERTED; BOTTOM: IS-2
BS-1 A/B	AXIS : HORIZONTAL;	2.17 cm	BUNDLE OF 9 ; CENTRAL CONDUCTOR HEATED

with a dissolving agent ("strip-ex", GC Electronics) , in order to obtain reference data without the large thermal impedance of the insulating coating ; (Designation : IS-1B) .

As the effect of the formvar appeared to be quite unusual in the first runs , an independent check of the sample design was conducted by instrumenting similar specimens and comparing the peak heat flux densities of nucleate boiling . Specimen IS-2 was mounted in a phenolic sample holder, as indicated in Figure IV. 3 . This specimen served as heating unit in the subsequent runs with dual-specimens (designated as DS-1A/B) . Specimen IS-3 had vacuum insulation . A duct system made out of brass was connected to the ends by soft soldering . Specimen IS-3A incorporated a Pt-10 % Rh heater, specimen IS-3B utilized again a constantan heater . Finally, a bundle of nine conductor sections with a central heating unit was assembled. Figure IV. 4 is a schematic of this specimen system (designated as BS-1 A/B).

In the first runs with the bundle (designated as BS-1A) the spacers were positioned horizontally. This configuration produces an initial heat transport by fluid convection in the horizontal direction. As long as He I is available near saturation, the vapor bubbles produced will eventually move toward the top of the dewar. In He II the entropy flow again is initially in horizontal direction. Subsequently , the entropy may be transported in radial direction (toward suitable heat sink locations if pressurized He II is used).

In the second series of runs the bundle spacers were positioned in vertical direction. In saturated He I any vapor bubble transport will be in the direction of the gravitational buoyancy force . In He II again initial entropy flow would be in vertical direction parallel to the spacers. Subsequent entropy transport is not necessarily upwards , in particular when an effective heat sink location is below the bundle while pressurized He II is used. (The designation of these runs is BS-1B).



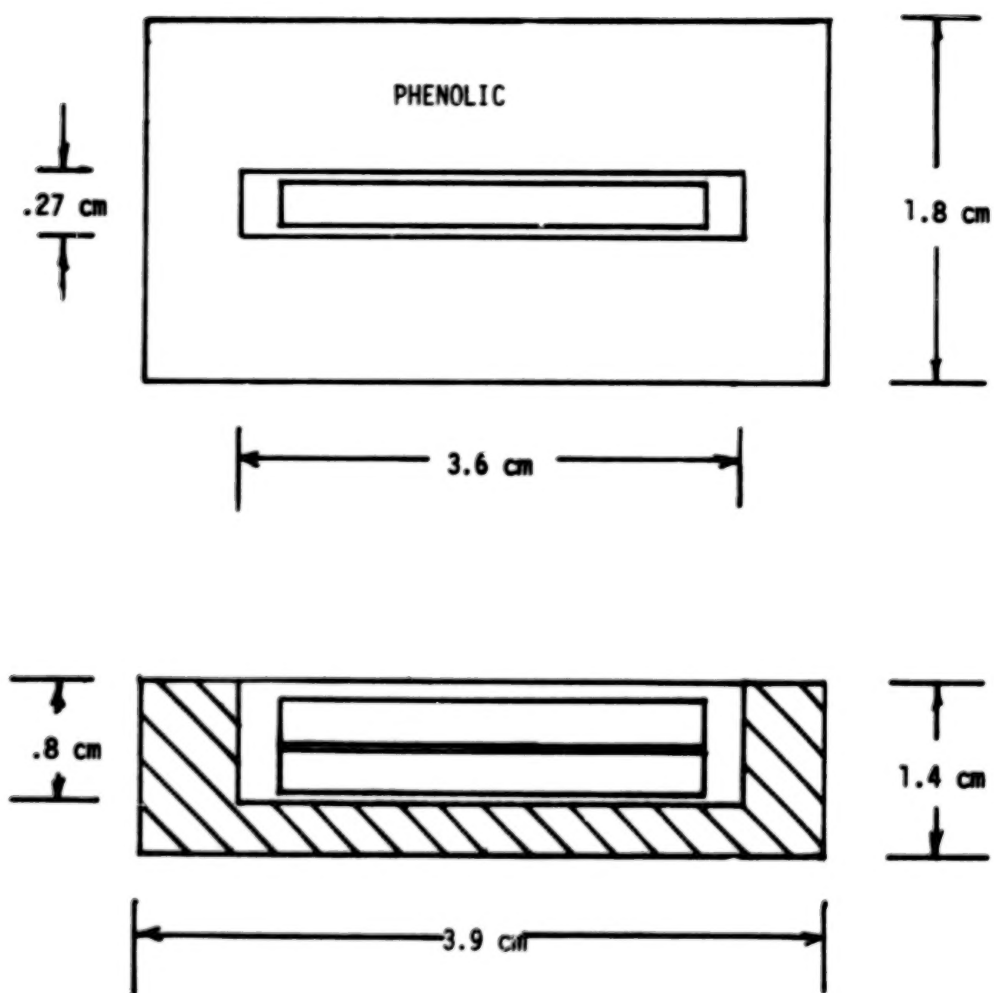


Figure IV. 3. Phenolic sample holder

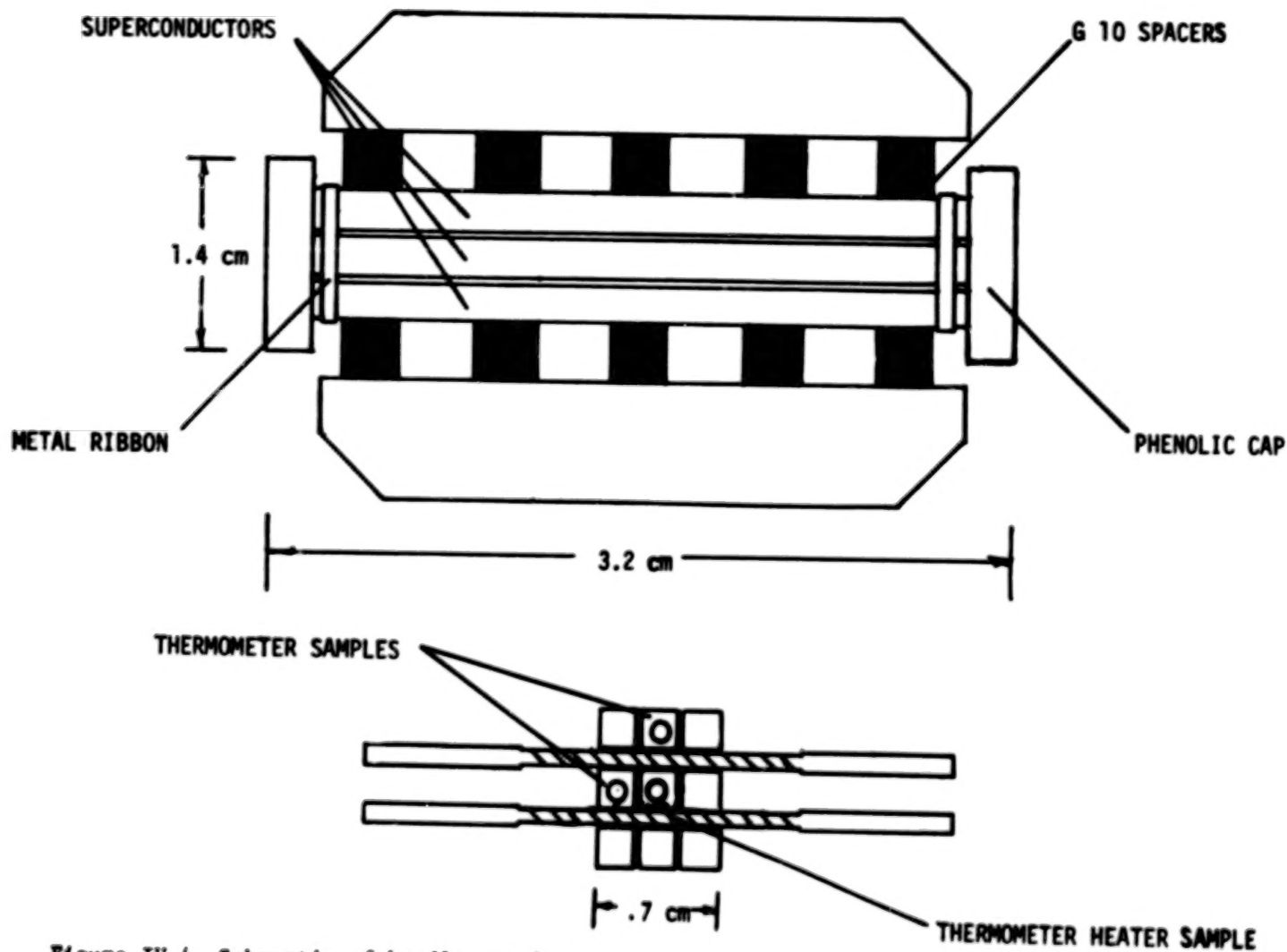


Figure IV.4. Schematic of bundle specimen

After specimen IS-1 had been instrumented , subsequent sample preparation tuned out to be quite lengthy and difficult with the small hole size selected . Therefore, the following specimens were machined with a larger drill of 0.14 cm O.D. ( 55 mil) . A few additional small-size holes had been manufactured early. These conductor pieces were used for thermometer samples in conjunction with the bundle specimen BS-1.

Figures IV.5 and IV.6 show the cross sections of the conductors used. Figures IV.7a and IV.7b are photographs of specimen BS-1.

Friction Apparatus. The setup used for the friction investigations consisted of a d.c. motor-drive unit , shaft ,load cylinder, friction rig, and heat flow meter. Figure IV.8 is a schematic of this assembly. The d.c. motor (12 V ; 1.4 A nominal rating) and associated gear box was located on top of the dewar flange outside the cryosystem. A stainless steel tube with an O.D. of 0.48 cm ( 3/16 in.) , and a wall thickness of 0.07 cm ( 28 mil) was used as shaft . Sealing was accomplished by a vacuum feed-through designed for relatively low rpm . It functioned satisfactorily in the angular speed range covered (up to about 16 rpm). Vacuum insulation was utilized around the outer portion of the interior friction apparatus. The test chamber communicated with the outer liquid He<sup>4</sup> bath (near saturation) via tubes of the heat flow A Gortler-Mellink device was used for the determination of the power dissipated during the friction runs .

The load cylinder was made out of brass . It could be displaced in vertical direction over a distance of about 0.8 cm. The mass of the brass cylinder assembly was 1.03 kg . This produced a specific load of  $1.97 \times 10^6 \text{ N/m}^2$  ( = 19.7 bar) . The vertical displacement was accomplished by a slit in the brass cylinder which decoupled the lower portion of the apparatus thermally from the "hot" upper assembly.

Figure IV.9 shows schematically the lower , central portion of the friction test chamber. 12 stainless steel tubes were used for the Gortler-Mellink heat flow meter; ( tube length : 3.3 cm , I.D. 0.0959 cm).

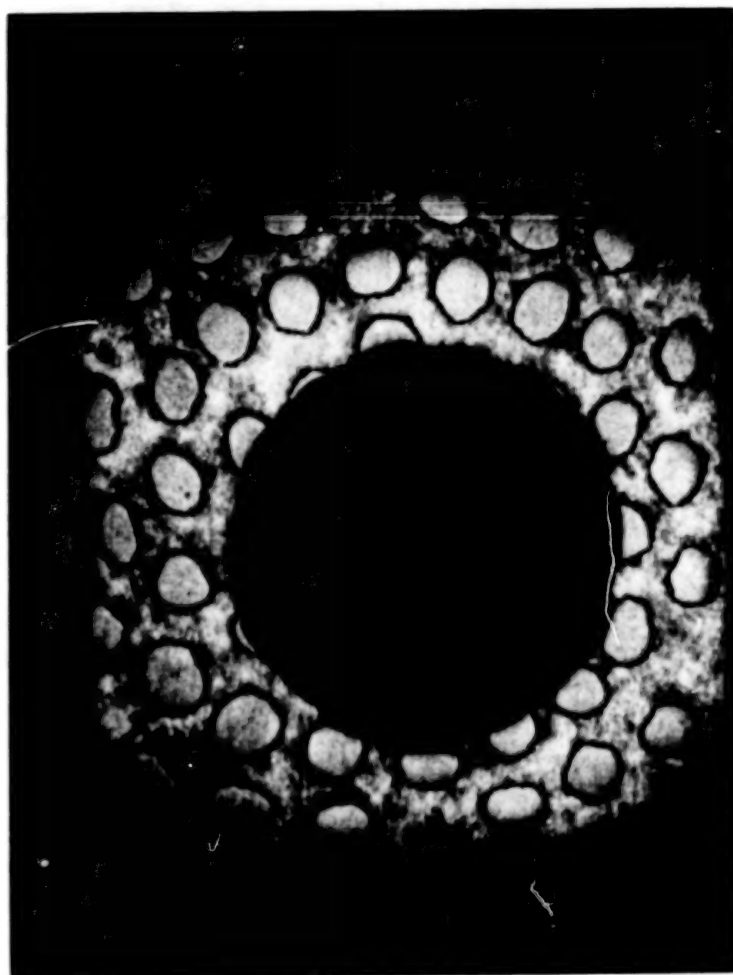


Figure IV.5 Specimen with hole of 0.117 cm dia.

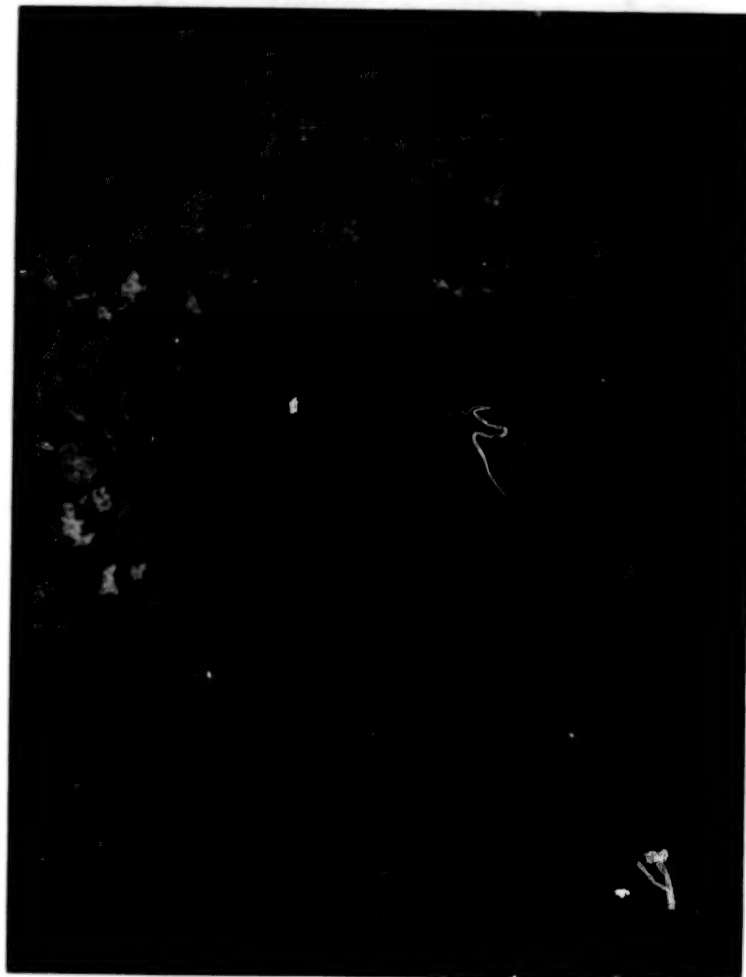
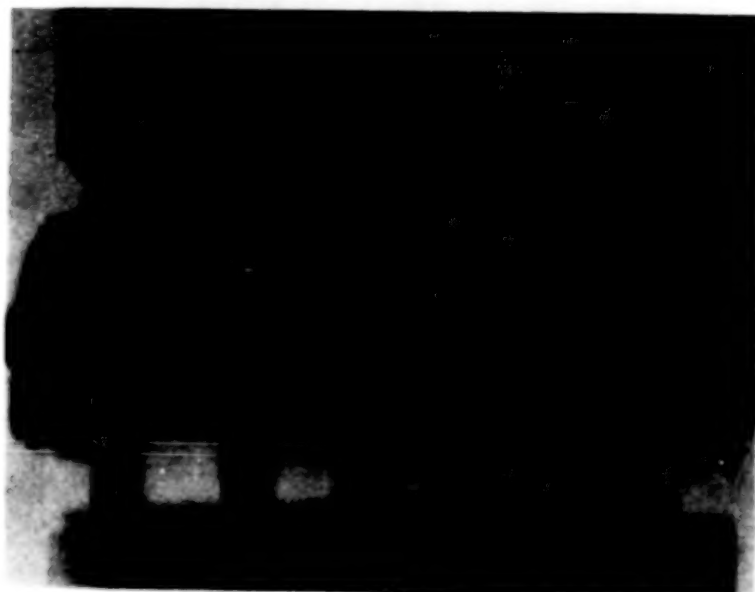
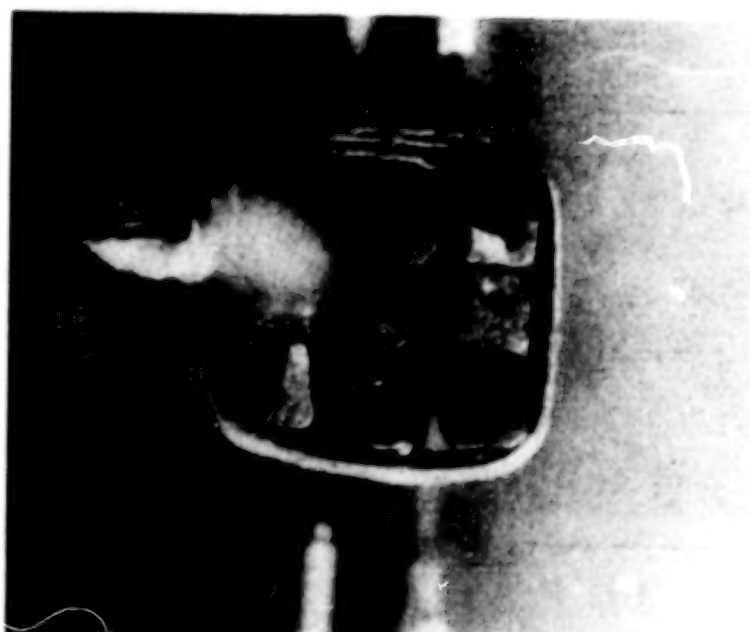


Figure IV.6 . Specimen with hole of 0.14 cm dia.



(a)



(b)

**Figure IV.7 . Photographs of bundle specimen BS-1**  
a. Side view  
b. Cross section

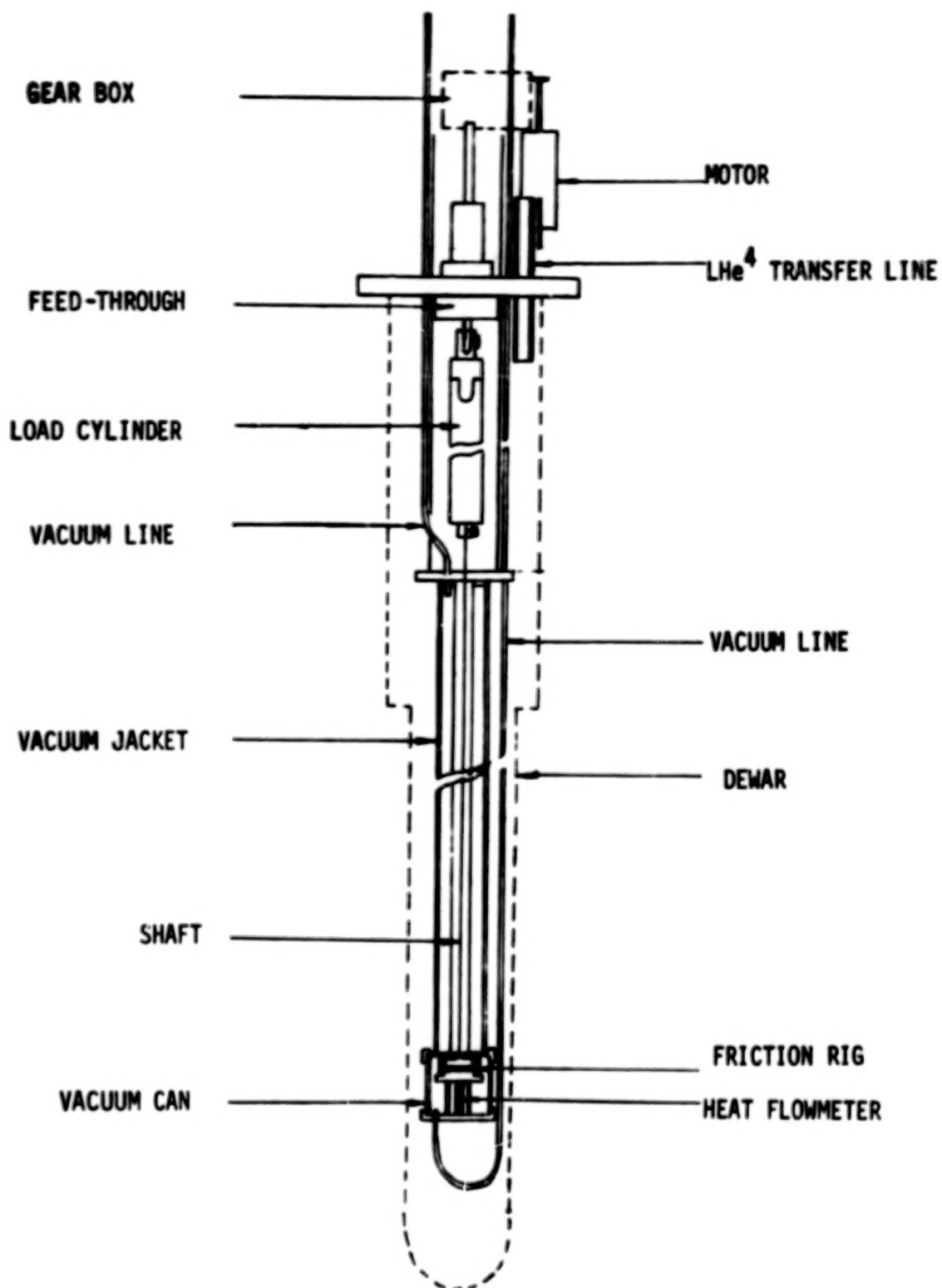


Figure IV.8 . Schematic of friction apparatus

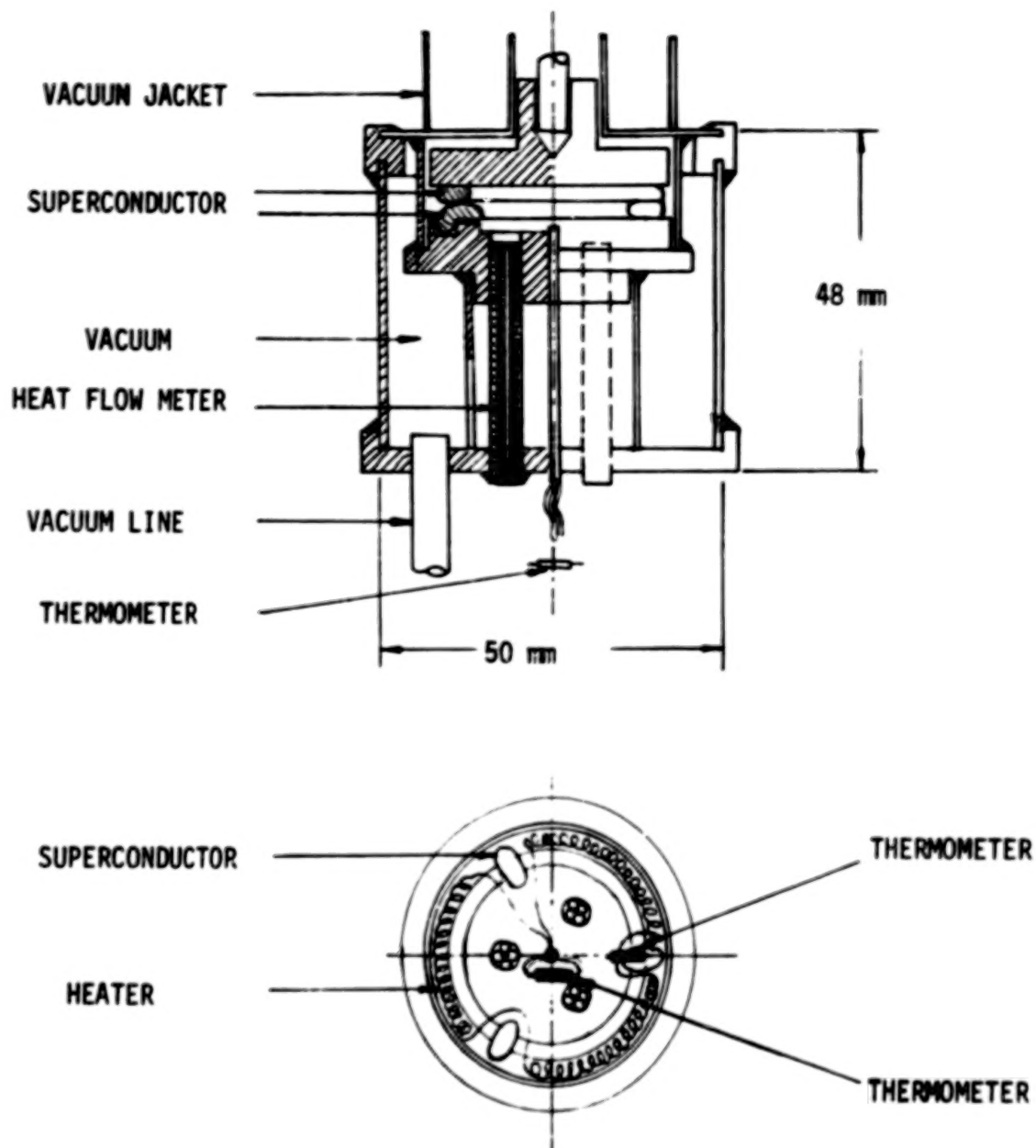


Figure IV.9 . Test chamber of calorimetric friction experiment



The upper rotating part contained at its lower end the ring-shaped formvar-insulated superconducting specimen. Three stationary sections of the same formvar-insulated conductor were located underneath the ring, as indicated in the Figure IV.9. A carbon thermometer measured the solid temperature of one of the segments. Another thermometer sensed the temperature of the liquid in the test chamber. The effective contact area between the formvar-coated parts was  $0.051 \text{ cm}^2$ .

Initially the heat flow meter was calibrated by energizing a heater mounted inside the test chamber. Results of this calibration are shown in Figure IV.10 as Gorter-Mellink parameter versus the bath temperature. The data are higher than the "ideal" function reported in Reference 15. It is noted though that various authors have obtained different Gorter-Mellink parameters with different insulated ducts. Figure IV.11 plots several transport results as  $A_{sn}^{1/3}$  versus the liquid bath temperature. The Gorter-Mellink quantity  $A_{sn}$  is written in terms of an effective counterflow velocity  $w_{eff}$  and a related heat flux density  $q$

$$q = \rho_s S T w_{eff} \quad (IV.1)$$

$$w_{eff} = [ S |\nabla T| / ( \rho_n A_{GM} ) ]^{1/3} \quad (IV.2)$$

( $\rho_s$  and  $\rho_n$  denote superfluid and normal fluid density respectively;  
 $S$  = entropy per unit mass ;  $A_{GM}$  = "fluidity" = reciprocal effective shear viscosity ).

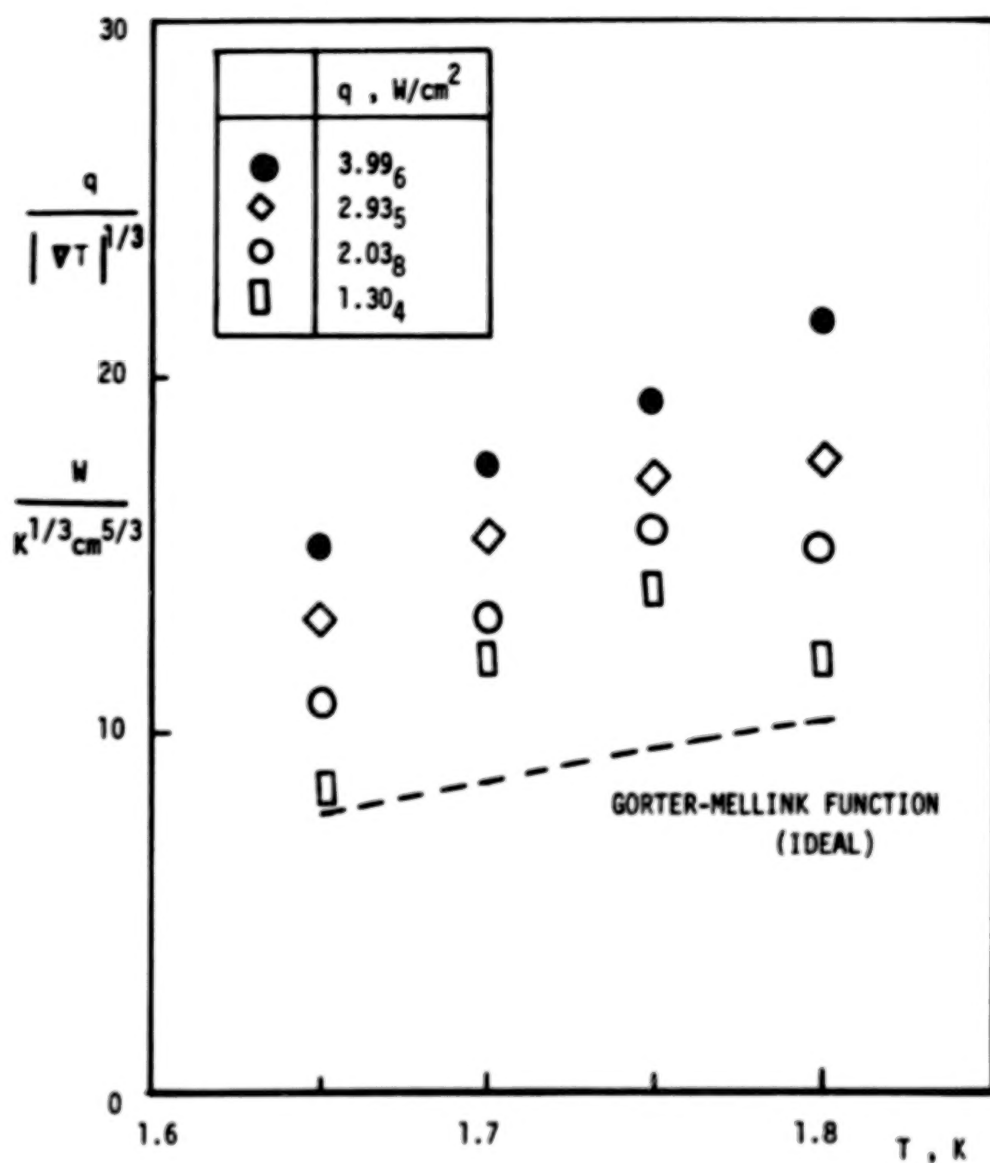


Figure IV.10 . Heat flow meter characteristics

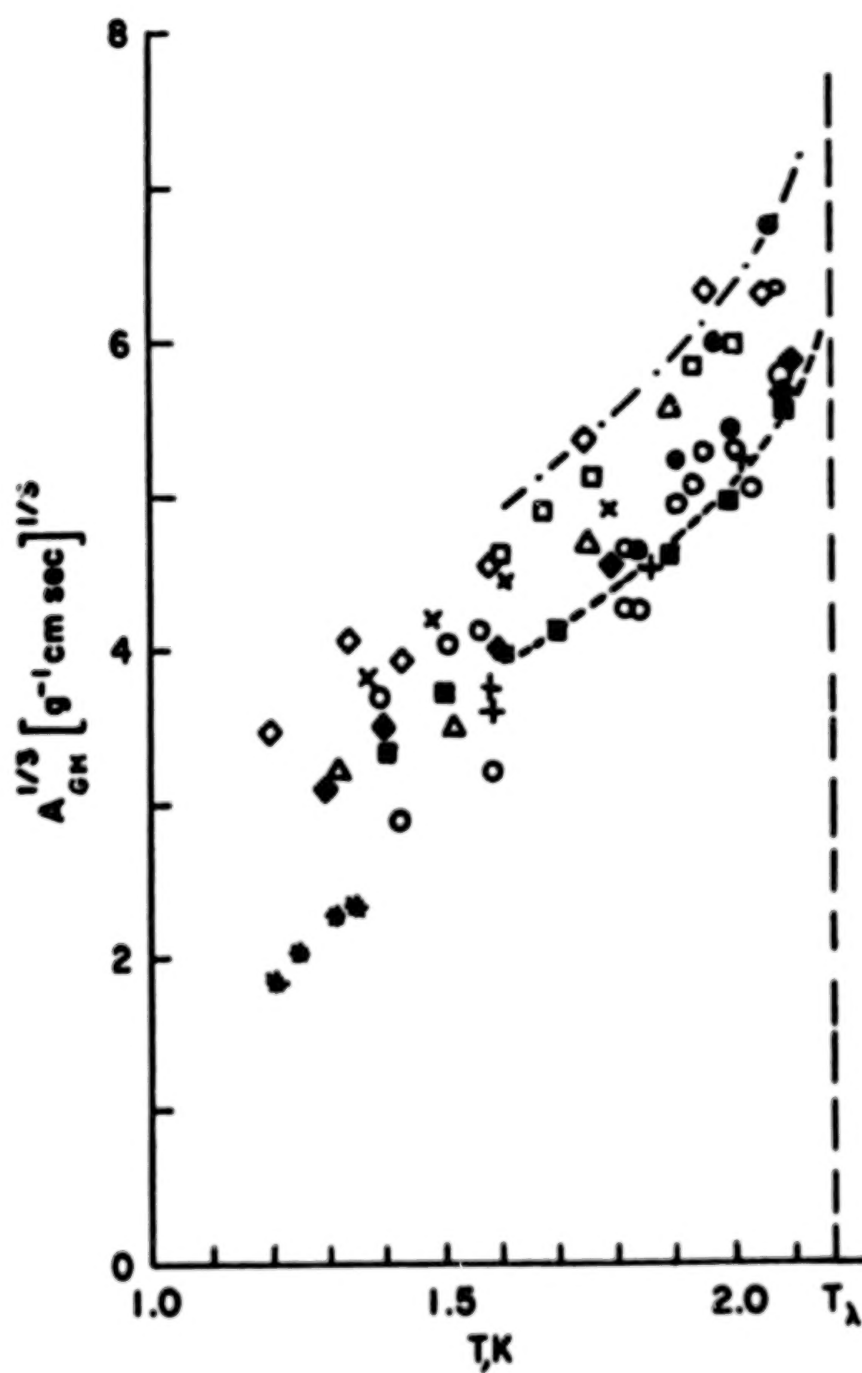


Figure IV.11 . Gorter-Mellink transport property  $A_{GM}^{1/3}$  versus  $T$

TABLE IV . 2

GORTER - MELLINK TRANSPORT STUDIES  
(LITERATURE DATA OF FIG. IV.11 )

	INVESTIGATOR(S)	SIZE (DIA. D.)	REFERENCE
□ × ◇	Keesom, Saris, Meyer	D=0.0346 cm 0.157	16
+	Kapitza	Glass Capillaries	17
△	Keesom-Duyckaerts	D - 0.00947 cm	18
◆	Vinen	Rectangular Cross Sec.	19
■	Chase	D = 0.08 cm	20
✱	Vicentini-Missoni Cunsolo	Apparatus with Electrodes	21
○	Chritchlow-Hemstreet	D = 0.1 to 1.0 cm	22
≡≡≡	Passow et al.	D = 0.1 to 1.0 cm	23
●	Linnet-Frederking	D = 0.45 cm (1 atm)	24

## V. RESULTS AND DISCUSSION

Various data have been obtained in the different areas of interest related to the interaction of the composite conductor with its coolant  $\text{He}^4$  in different thermodynamic states. The investigations have been conducted with single specimens and with conductor assemblies. Turning first to the individual conductor characteristics we do not follow the chronological sequence. Instead, quantities of prime importance for the data reduction are considered first. An example is the thermal conductivity of the organic insulation, and the peak heat flux density in near-saturated liquid. The latter permits some insight into the performance characteristics of different specimen designs. Further, the quench-onset data are included in this discussion.

Subsequent to the individual conductor discussion, a survey of heat capacity information is given, as the experimental program did not include detailed runs. In addition, the performance of the conductor assembly is an important part of the magnet design information. Dual-conductor specimens have been investigated which allowed conclusions concerning the thermal conductivities of the solid system. Further, the conductor-spacer assembly of several specimens is more closely tied together with the performance of the components in an actual magnet. This point is discussed as the last item of the thermal solid-coolant interaction. The final topic considered is the friction between formvar-coated conductors.

In the next Section V.A the individual specimens are considered primarily. However, an exception in the thermal conductivity discussion is the use of dual-specimens. The latter permit valuable insight into various thermal resistances related to the solid state.

## V . A . THERMAL DATA OF INDIVIDUAL SPECIMENS

### 1 . THERMAL CONDUCTIVITY RESULTS

The thermal conductivity of formvar was evaluated from two different specimens. As most organic coatings have a rather small thermal conductivity, even a thin layer of insulation may have a pronounced influence upon the post-quench performance. The nominal thickness listed in Table II.1 has been inserted in the data reduction.

The dual specimen setup DS-1A was used to obtain overall temperature differences from the lower heated conductor to the upper unheated conductor equipped with a thermometer (Figure IV. 3). The entire thermal resistance of this assembly is the sum of two Cu-Type II resistances two formvar layer resistances and a liquid film resistance . Additional contact resistances may not be entirely negligible at low T. However, the two metal resistances and the thin liquid film resistances appear to be negligible compared to the geometry uncertainty of the formvar coatings. Therefore, at sufficiently high T , the thermal conductivity (k) has been evaluated from an extrapolation of measured  $q (\Delta T)$  - functions. The equation used is

$$k = \lim_{\Delta T \rightarrow 0} \left[ (q / \Delta T) \right] \cdot d_{FV} \quad (V.1)$$

The various results obtained are listed in Table V.1 . Figure V.1 plots the data versus T .

The second set of data has been deduced from runs with the specimen IS-3. After heat leak corrections the thermal conductivity was deduced as mean value k from data in the nucleate boiling regime . As the thermal resistance of the latter is finite, but relatively small (up to

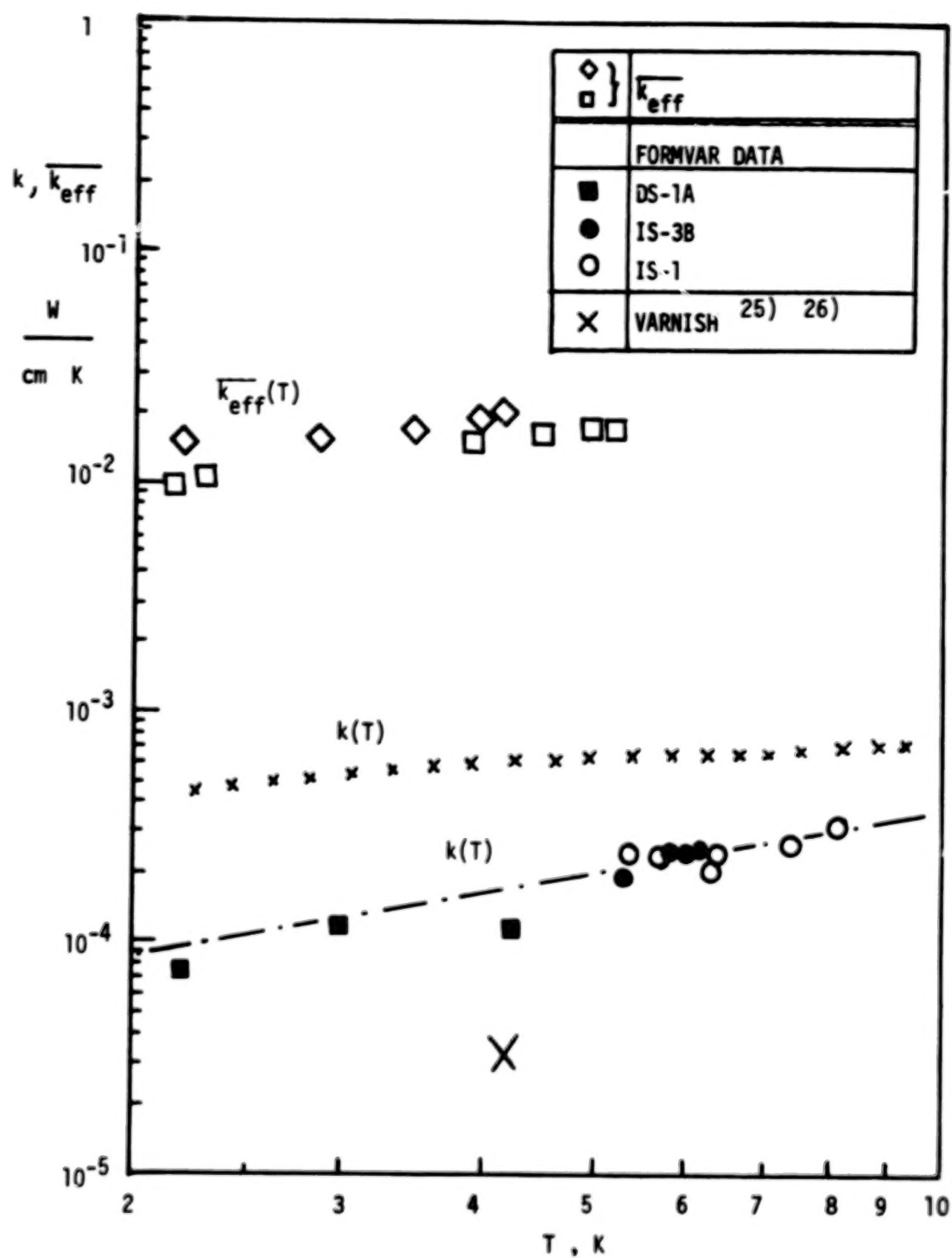


Figure V. 1 . Thermal conductivities

25 % ) the data incorporate the usual uncertainty resulting from variations in the  $\Delta T$ -values of nucleate boiling. The  $\bar{k}$ - results are listed again in Table V.1 and in Figure V.1. A few values in the He II regime at temperatures close to  $T_\lambda$  ( where the Kapitza conductance is high ) are included. A least square fit for specimen IS-3 is

$$\bar{k} = 6.9 \times 10^{-5} \cdot T^{0.70} \quad ( V.2 )$$

( $\bar{k}$  in  $W \text{ cm}^{-2} \text{ K}^{-1}$  ,  $T$  in K ). A third set of data has been deduced from specimen IS-1 using the same procedure as for IS-3 ; (Data in Table V.1) . The entire set of data is described on the basis of the least square fit

$$\bar{k} = 4.9 \times 10^{-5} T^{0.89} \quad ( V.3 )$$

(Same set of units as in Equation IV.2) .

The thermal conductivity of G 10 spacers has been deduced from runs with specimen DS-1B. This specimen uses the same elements as DS-1A (heater at the bottom , thermometer sample at the top in contact with bulk fluid) . The spacer was inserted between the lower and the upper composite conductor element. Evaluation proceeded along the lines of Equation ( V.1) on the basis of the spacer thickness  $d = 0.038_1 \text{ cm}$  .

In addition results obtained with specimen IS-1B (without form-var coating) were used to calculate an effective thermal conductivity  $\bar{k}_{\text{eff}}$  . This quantity is representative of the overall thermal resistance of the type II- Cu material , in particular its interior boundary domain near the hole wall . Further, it incorporates the fluid boundary layer between surface and bulk fluid. This contribution may include a contact resistance at the metal-fluid boundary. In particular , in He II the overall boundary resistance is a complex quantity affected by the oxide layer thickness at the Cu-surface. The surface appeared to be reasonably shiny after rinsing with acetone, (similar to the uncoated material).



For the evaluation the following equation for a cylindrical geometry was used :

$$q = \dot{Q} / (2\pi R_o L) = \frac{\overline{k_{eff}} \cdot \Delta T}{R_o \cdot \ln(R_o/R_i)} \quad (V.4)$$

This reference heat flux density is based upon an equivalent diameter ( $2R_o$ ) = 0.220 cm .  $R_o$  and  $R_i$  denote the equivalent outer radius and the inner (hole) radius respectively.  $L$  is the length of the test section of the specimen. After insertion of numerical values , Equation ( V.4) may be expressed as

$$q = 14.4 \cdot \overline{k_{eff}} \cdot \Delta T \quad (V.5)$$

( $q$  in  $W\ cm^{-2}$  ,  $\overline{k_{eff}}$  in  $W\ cm^{-1}\ K^{-1}$  ,  $\Delta T$  in  $K$  ) .

Figure V.1 plots the  $k_{eff}$ -data versus  $T$ . The results are one order of magnitude below the values for  $k$  in radial direction of a Cu-NbTi composite. The present  $k_{eff}$ -data are lower bounds to the metal -type II thermal conductivity in radial direction, as they include the system Cu-type II - contact resistances- boundary layer of the fluid. Further,  $k_{eff}$  is two orders of magnitude above the values obtained for formvar.

The formvar-data of the present runs are seen (Fig. V.1) monotonically increasing function of  $T$  . For a comparison , another organic insulator has been considered , ( a polyvinyl phenolic known as GE varnish 7031). Several investigators have reported data for this material (Refs. 25 , 26 , 27 ). The majority of the varnish data are above the present formvar results. We note however that a few data have been reported which are substantially lower than the present formvar results.

TABLE V.1  
THERMAL CONDUCTIVITY

A. Formvar: Run DS-1A, 92177

T, K	k , W cm <sup>-1</sup> K <sup>-1</sup>
4.20	1.11 x 10 <sup>-4</sup>
3.00	1.14 x 10 <sup>-4</sup>
2.20	7.26 x 10 <sup>-5</sup>

B. Formvar: Run IS-3B, 90477

6.38	2.52 x 10 <sup>-4</sup>
6.25	2.63 x 10 <sup>-4</sup>
6.03	2.55 x 10 <sup>-4</sup>
5.78	2.49 x 10 <sup>-4</sup>
5.58	2.26 x 10 <sup>-4</sup>
5.38	1.91 x 10 <sup>-4</sup>

C. Formvar: Run IS-1

8.12	3.37 x 10 <sup>-4</sup>
7.41	2.79 x 10 <sup>-4</sup>
6.35	2.05 x 10 <sup>-4</sup>
5.82	2.63 x 10 <sup>-4</sup>
5.76	2.73 x 10 <sup>-4</sup>
6.38	2.60 x 10 <sup>-4</sup>
5.78	2.37 x 10 <sup>-4</sup>
5.35	2.72 x 10 <sup>-4</sup>

TABLE V.1  
THERMAL CONDUCTIVITY

D. G-10 spacers: Run DS-1B, 92277

T, K	k, W cm <sup>-1</sup> K <sup>-1</sup>
2.17	6.35 x 10 <sup>-4</sup>
2.20	1.41 x 10 <sup>-3</sup>
3.00	3.04 x 10 <sup>-3</sup>
4.20	1.73 x 10 <sup>-3</sup>

E. Composite, radial direction: Run IS-1B,

	k <sub>eff</sub> , W cm <sup>-1</sup> K <sup>-1</sup>
2.20	1.56 x 10 <sup>-2</sup>
2.32	1.60 x 10 <sup>-2</sup>
2.92	1.60 x 10 <sup>-2</sup>
3.51	1.83 x 10 <sup>-2</sup>
3.97	2.08 x 10 <sup>-2</sup>
4.20	2.09 x 10 <sup>-2</sup>
(above conductivity calculated using q <sub>p</sub> )	
2.20	9.5 x 10 <sup>-3</sup>
2.32	1.0 x 10 <sup>-2</sup>
2.92	1.5 x 10 <sup>-2</sup>
3.51	1.8 x 10 <sup>-2</sup>
3.97	1.8 x 10 <sup>-2</sup>
4.20	1.8 x 10 <sup>-2</sup>
(above conductivity calculated using q <sub>R</sub> )	

An assessment of the lower bound to the  $k_{\text{eff}}(T)$ - function involves a complex system of thermal impedances. The metallic composite appears to be sensitive to local deformation and damage at the inner hole surface. If the electronic mean free path is large enough , boundary scattering at the type II - Cu interfacial domain may be a contributing factor. This point, however should not be of concern when the mean free path in the Cu is reduced significantly due to local damage.

Very little appears to be known about the entropy carriers at the Cu-formvar interface . Two recent studies (References 13 and 14 ) have been devoted to the thermal boundary resistances at metal-epoxy interfaces. According to Reference 13 , the heat transfer coefficient is a monotonically increasing function of the temperature . Reference 14 reports data for a copper - epoxy - copper sandwich . They suggest that the apparent thermal boundary resistance at the interfaces may be a factor of 100 larger than calculated by straightforward theories of the acoustic mismatch in impedances of the two materials.

## V. A.2. PEAK HEAT FLUX DENSITIES

Peak heat flux densities occur at various phase transitions from one fluid condition to another. These changes of state include the conversion of near-saturated He I and He II into vapor at local hot spots, the transition from subcooled liquid to vapor, from He II to He I at pressures above and below the critical pressure ( $P \gtrless P_c$ ). An additional quantity of considerable concern for most conservative sizing of copper layers for post-quench scenarios is the recovery heat flux density ( $q_R$ ). We turn first to the peak flux density ( $q_p$ ) of the transition from near-saturated liquid to vapor.

Figure V.2 plots the results  $q_p(T)$  obtained with near-saturated liquid. Various data for He I follow qualitatively the equation of Kutateladse (Reference 29). At the lambda temperature ( $T_\lambda$ ),  $q_p$  has a low value, about 50 % of the highest  $q_p$  encountered. As  $T$  is raised,  $q_p$  increases monotonically toward a maximum  $(q_p)_{\max}$ . At temperatures beyond 4 K,  $q_p$  starts to fall rapidly toward very low values at the critical temperature ( $T_c$ ). The Kutateladse function predicts  $q_p = 0$  at this point. The theoretical equation may be expressed as

$$q_p = 0.16 (\rho_v \lambda) v_{\text{eff}} \quad (\text{V.6})$$

$$v_{\text{eff}} = (gB)^{1/2} \left\{ (\rho_L - \rho_v) / \rho_v \right\}^{1/2} \quad (\text{V.7})$$

$$B = \left\{ \sigma / [(\rho_L - \rho_v) g] \right\}^{1/2} \quad (\text{V.8})$$

( $\rho_v$  and  $\rho_L$  denote the densities of saturated vapor and liquid respectively,  $g$  = gravitational acceleration,  $\lambda$  = latent heat of vaporization,  $\sigma$  surface tension between liquid and vapor,  $B$  = characteristic bubble size).

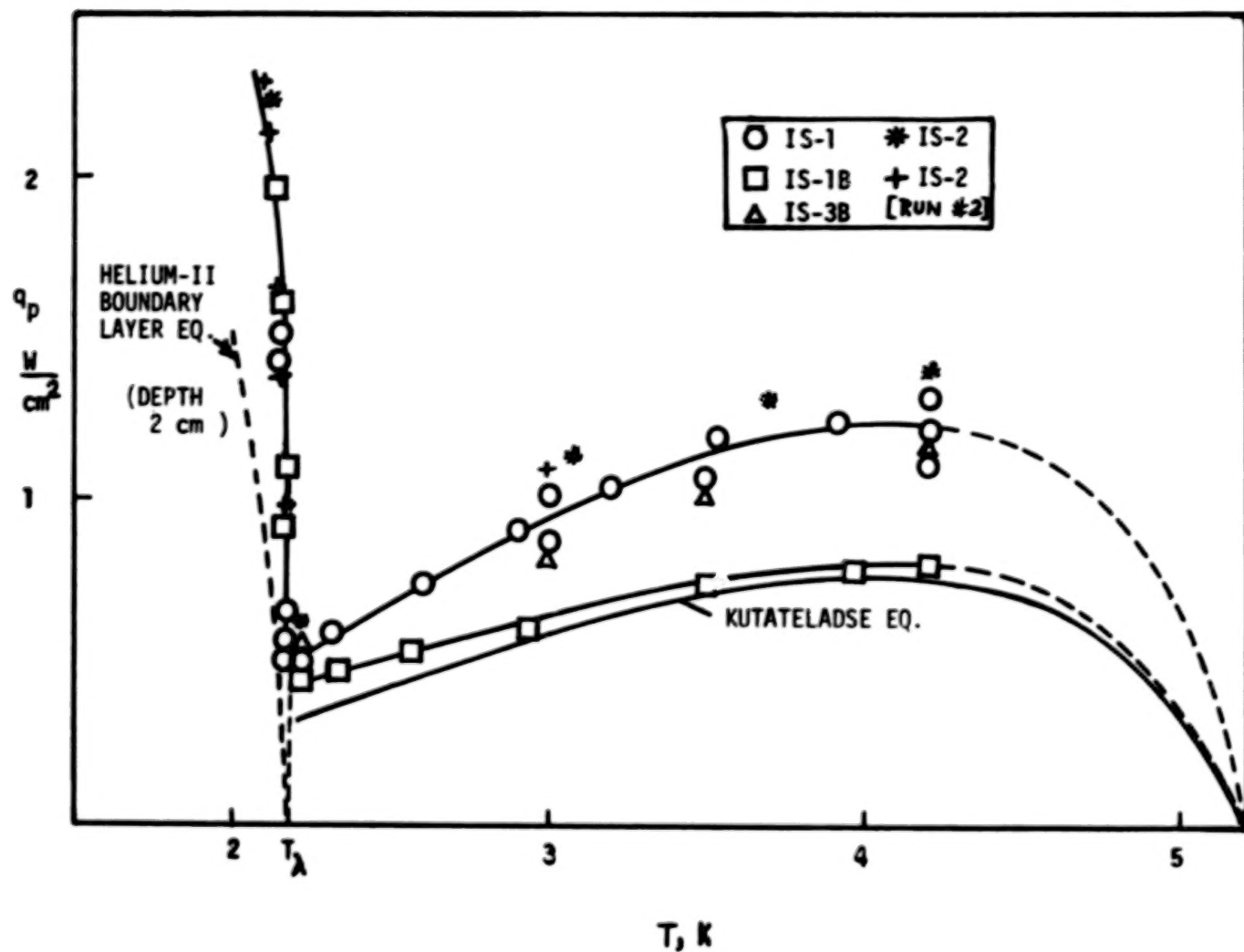


Figure V.2 . Peak heat flux densities  $q_p(T)$

In Figure V.2 shows that only the data of the bare specimen IS-1B are in close quantitative agreement with the Kutateladse function. All other results obtained with formvar-insulated specimens are higher. A considerable heat leak correction has been applied to the raw data for specimen IS-3B. This specimen has two major heat leak contributions . First, the vacuum line connections (made out of brass) constituted a solid state heat leak. Second another metallic heat leak was created by attaching the current leads to the specimen . As a separate series of heat leak runs ( with the heat transfer surface insulated) , has been conducted, this heat leak was known quite well. It amounted to about 30 % at most temperatures.

Influences of insulating coatings are discussed in some detail in the next Section V. A.3 . Therefore, we remark at this point only that several authors have observed increases in  $q_p$  . A number of factors may be responsible for this rise . One possibility is the change of the bubble frequency by a change in the thermal penetration during temperature cycling associated with bubble growth. Another point may be the existence of a stronger axial component of the heat flux density vector. No microscopic details appear to be known today. Therefore we refrain from a detailed discussion of controversial interpretations. Certainly the changes in roughness (micro-roughness) and adsorbed foreign impurity content may be variables to be considered in any detailed micro-study.

In the He II range of T a drastic increase is seen in Figure V.2 The peak heat flux density appears to be a monotonically increasing function of the difference between T and the bath temperature. At relatively low T no data could be obtained with some reliability , as the large (absolute) power appeared to present difficulties with the existing pumping system. This point was quite apparent at pressures above the saturated vapor pressure. Three heat transfer correlations for the He II boundary layer have become known in recent time: (1) the Haben et al. equation (Reference 30); (2) Leonard-Clermont correlation (Reference 31) , and (3) , the Soloski Equation (Reference 32 ). The first equation has been based upon a rather

rather limited amount of data available at the time of publication. The equation may be written in the following form for the flat plate:

$$q = \rho_s S T w_{\text{eff}} \quad (\text{V.9})$$

$$w_{\text{eff}} = C_{\text{HC}} \left\{ (S \Delta T / L_{\text{Ref}}) (\eta_n / \rho) \right\}^{1/3} \quad (\text{V.10})$$

As this equation has been based upon the limiting temperature difference available in saturated liquid He II, the limiting  $\Delta T$ -value has to be inserted to obtain  $q_p$ ; ( Properties evaluated at the arithmetic mean temperature of the He II boundary layer).;  $\eta_n$  = normal fluid viscosity,  $S$  entropy per unit mass,  $\rho_s$  superfluid density =  $(\rho_s/\rho) \rho$ ;  $C_{\text{HC}}$  = const of the Haben et al correlation. We note that this first equation has been quite useful for early predictions. However it is not entirely consistent with the present form of other zero net mass flow cases (e.g. Gorter-Mellink thermomechanical convection).

The Leonard-Clermont equation is considered in the asymptotic limit of size-independent heat flux densities  $q$ . The modified asymptote of Amar ( Reference 42) is expressed as

$$q = \rho_s S T w_{\text{eff}} \quad (\text{V.11})$$

$$w_{\text{eff}} = C_{\text{LC}} \left\{ (S \Delta T / L_{\text{o,R}}) \cdot (\eta_n / \rho_s) (\rho / \rho_n)^2 \right\}^{1/3} \quad (\text{V.12})$$

( $L_{\text{o,R}}$  is a constant reference length equal to  $L(T)\rho/\rho_s$ ;  $\rho_n$  = normal fluid density  $(\rho_n/\rho) = 1 - (\rho_s/\rho)$ ;  $C_{\text{LC}}$  = const ). An apparent difference between Equations ( V.10) and ( V.12) is the appearance of the normal fluid density. The Haben et al. correlation has been adopted only for the vicinity of the maximum in  $q_p$  to the vicinity of  $T_\lambda$ . Low temperatures have been excluded. In contrast, the Leonard-Clermont Eq. appears to be a useful first order approach to the entire range of  $T$  for



which data are available (down to about 1 K) . Again the equation is to be used for the limiting  $\Delta T$ -value at the liquid vapor phase equilibrium curve . According to Amar's asymptotic equation (Reference 42 ) the thermo-physical properties are to be evaluated at the arithmetic mean temperature of the He II boundary layer .

The correlation proposed recent  $\tau$  by Soloski (Reference 32) may be written as

$$q = \rho_s S T w_{eff} \quad (V. 13)$$

with an effective (relative ) velocity)

$$w_{eff} = K_{SC} (\rho_s/\rho_n)^{1/3} \left\{ (\eta_n/\rho) S |\nabla T| \right\}^{1/3} \quad (V. 14)$$

The constant  $K_{SC} = 9.28$  has been used in conjunction with a reference length in the  $|\text{grad } T|$  - term of  $L_R = 1 \text{ cm}$  ; (Properties evaluated at the arithmetic mean temperature of the He II boundary layer ) . Again the equation is most useful for the limiting  $\Delta T$  accessible to the He II. In He II below the lambda pressure of saturated liquid,  $\Delta T$  is the difference between the value at the phase boundary of vapor-liquid equilibrium and the local bulk value . In pressurized He II above  $P_{\lambda, \text{sat}}$ ,  $\Delta T$  is the difference between the lambda curve and the bulk value . This latter case usually requires integration of the thermohydrodynamic equations ( e.g. V.13 and V.14) when the condition  $\Delta T \ll T$  is not met . In Figure V.2 the function (V.13) for the maximum  $\Delta T$  ( when  $q \rightarrow q_p$ ) has been included for a small submersion depth of 2 cm . This function is a lower bound to the data , as most of the runs were conducted at depths of the order 10 cm . ( Another simplification is the use of the liquid bulk temperature for the determination of the theoretical function ; At 2 cm depth , the peak value of  $\Delta T$  is not very large , and  $\Delta T \ll T$  above  $T = 2 \text{ K}$  ). As the submersion depth changes ( due to a decrease of the liquid level during the runs),  $q_p$  is predicted to vary by more than a factor of 2 (according to Eq. V.13), for depths from 10 cm to 2 cm.

The "peak phenomenon" is the result of thermal switching from one single-phase regime to another two-phase regime. The latter usually has a lower heat transfer coefficient due to the presence of a more disordered phase (with higher entropy). Upon power reversal ( $dq < 0$ ) a minimum heat flux density may be attained. This implies "recovery" of the superconducting state in the context of the present heater simulation phenomena. Thermal switching depends upon the choice of the thermodynamic state of the fluid. Examples are discussed below. We consider first the phenomena of near-saturated liquid conditions.

In the example Figure V.3 the transitions are clearly visible as sharp changes of the temperature. This figure is a plot of the non-linear temperature signal (recorded as voltage of the carbon resistance thermometer) versus heater current  $I$ . As the power is increased from zero to finite values ( $dq > 0$ ), an initial regime of transient conduction to natural convection is observed. Subsequently, vapor bubble generation during nucleate boiling keeps the solid surface temperature relatively close to the bath temperature. At the peak heat flux a drastic increase in  $T$  accompanies the onset of film boiling. Upon power reversal the sample stays in the film boiling regime until a sharp reduction in  $T$  signals recovery to nucleate boiling temperatures. The  $T$ -values during  $dq < 0$  in the nucleate boiling regime are lower than for  $dq > 0$ . This indicates that fully established bubble generation may be responsible for the difference. Figure V.3 represents the behavior of the uninsulated specimen IS-1B which is at relatively low  $T$  during nucleate boiling. In contrast, records of formvar-coated samples showed very large temperature excursions into a temperature range with limited resolution available from the present carbon thermometry.

Figure V.4 is a plot of recovery results  $q_R(T)$ . The lowest  $q_R$ -values are seen to occur with the bare specimen IS-1B. The formvar-coated specimen IS-1 has a considerably larger  $q_R$ . Specimens with partial contact with insulating walls (e.g. IS-2C) did not show a large difference between  $q_p$  and  $q_R$ . Figure V.4 includes a theoretical function for the

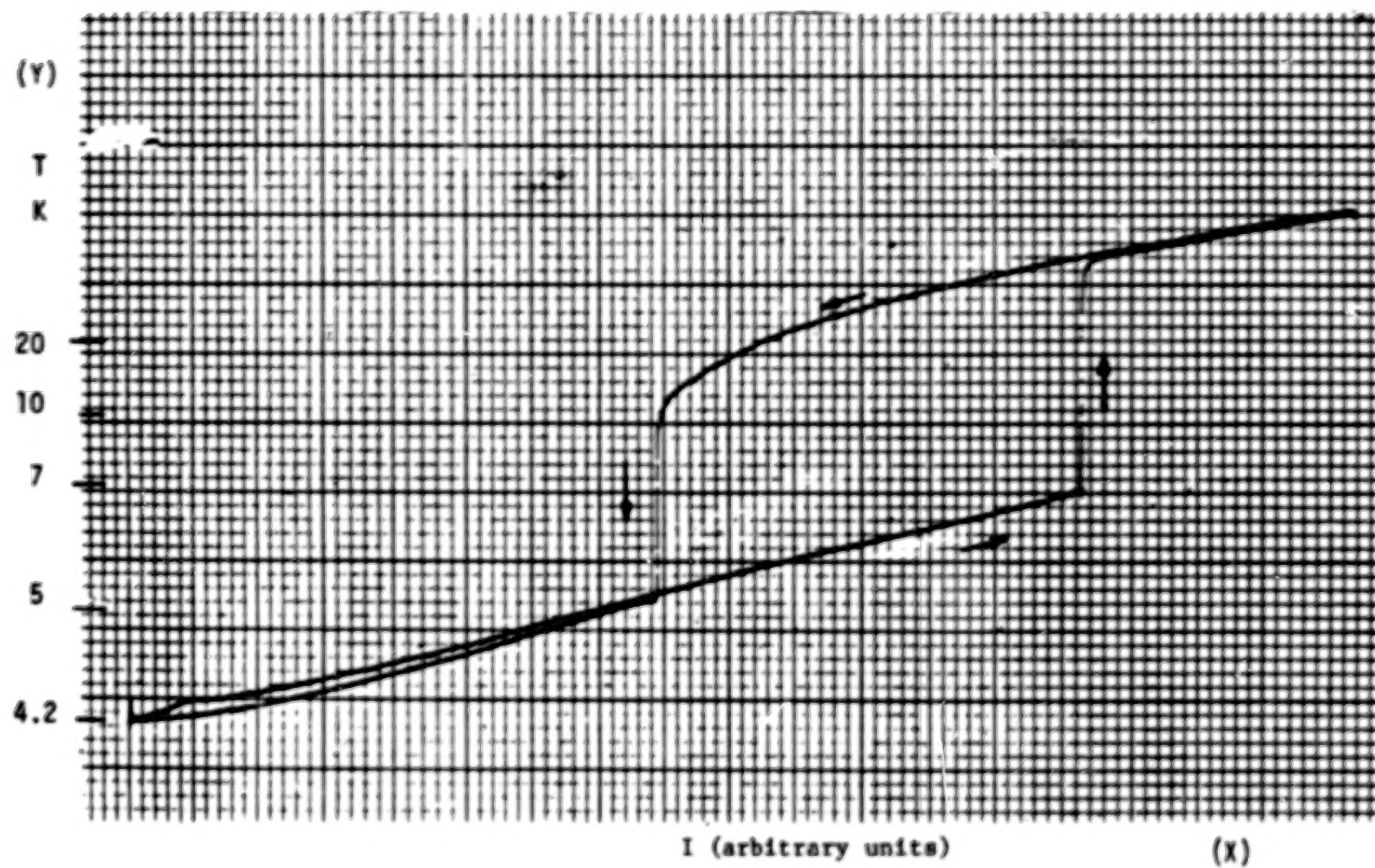


Figure V.3 . X-Y-plotter record for specimen IS-1B ; (Y = thermometer signal;  
X = heater current

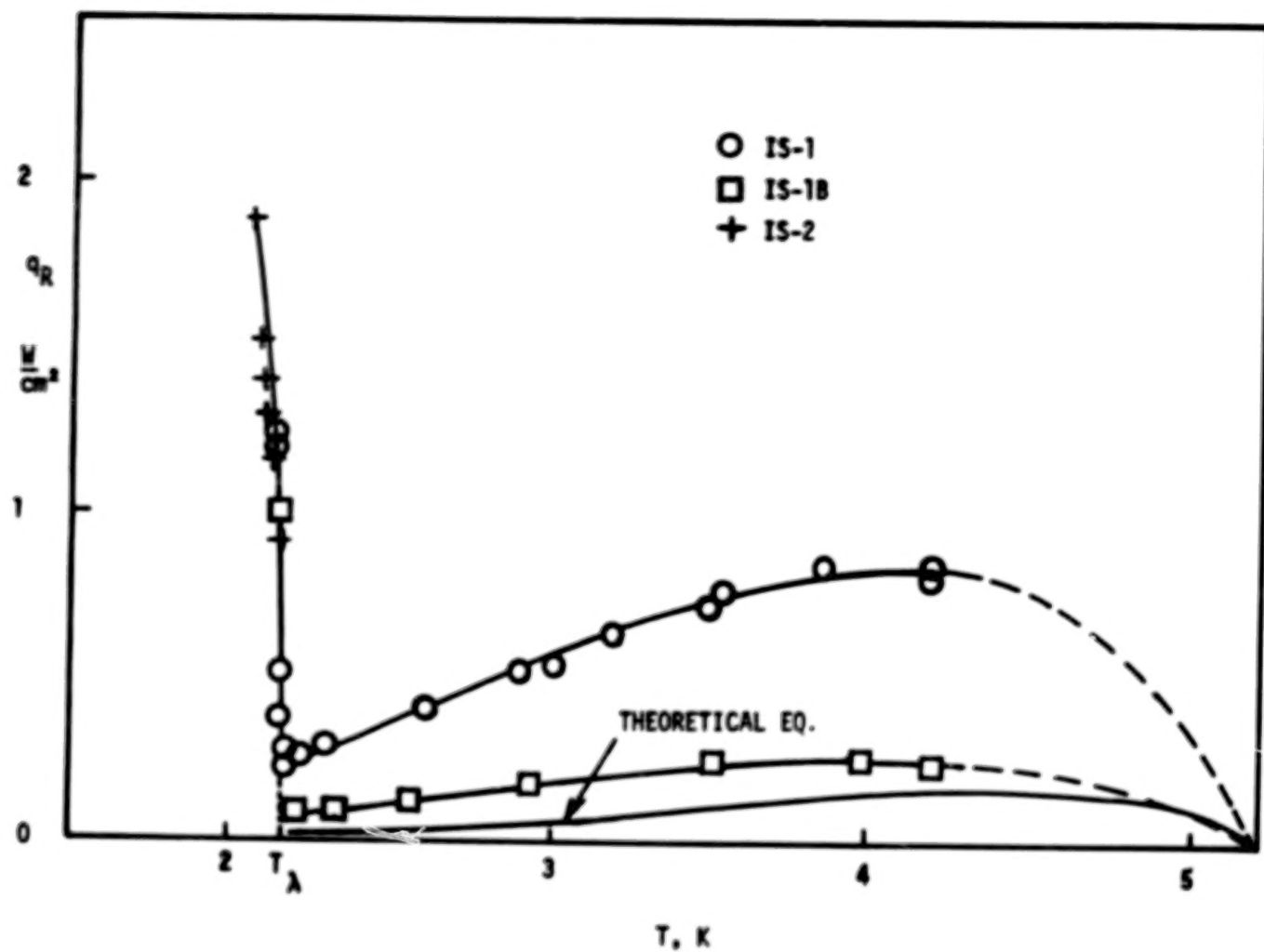


Figure V.4 . Heat flux densities at recovery  $q_R(T)$

recovery values which are usually referred to as "minimum heat flux densities" of film boiling (Reference 33) . This function is seen to be lower than the experimental data obtained in the present runs. More specifically , the following theoretical function has been used in Figure V.4

$$q_R = 0.09 \rho_v \lambda \cdot \left\{ \epsilon_g (\rho_L - \rho_v) / (\rho_L + \rho_v)^2 \right\}^{1/4} \quad (V.15)$$

Examples with runs with pressurized cryo-fluid  $\text{He}^4$  are presented in Figures V.5 and V.6 ; (Y = non-linear temperature signal, X = heater current in arbitrary units). Figure V.5 is a plot at  $P < P_c$  at a bath temperature of  $2.11_4$  K. There are two hysteresis loops : The first one is initiated at the transition from He II to He I . A sharp change toward larger T signals the appearance of the He I phase at a limiting heat flux density  $q_\lambda$  . Upon further heat supply to the fluid a second transition from liquid to vapor takes place. Details of the transition phenomena are not completely clear. However eventually a complex state of film boiling accompanied by the presence of two liquid phases is established. Upon power reversal to  $dq < 0$  , sharp reductions in T indicate recovery of two-phase liquid conditions, and eventually recovery of single phase He II conditions.

Figure V.6 for  $\text{He}^4$  above the thermodynamic critical pressure shows only one pronounced hysteresis loop. At the excursion to high T a well-defined limiting heat flux density  $q_\lambda$  is retained . This transition is the He II - He I phase change (in the presence of heat flow). In principle another transition at the transposed critical curve should occur with a deterioration in heat transfer rates . This effect could not be detected in the present runs. Upon power reduction ( $dq < 0$ ) again a sharp change in the derivative is observed at the recovery of He II temperatures.

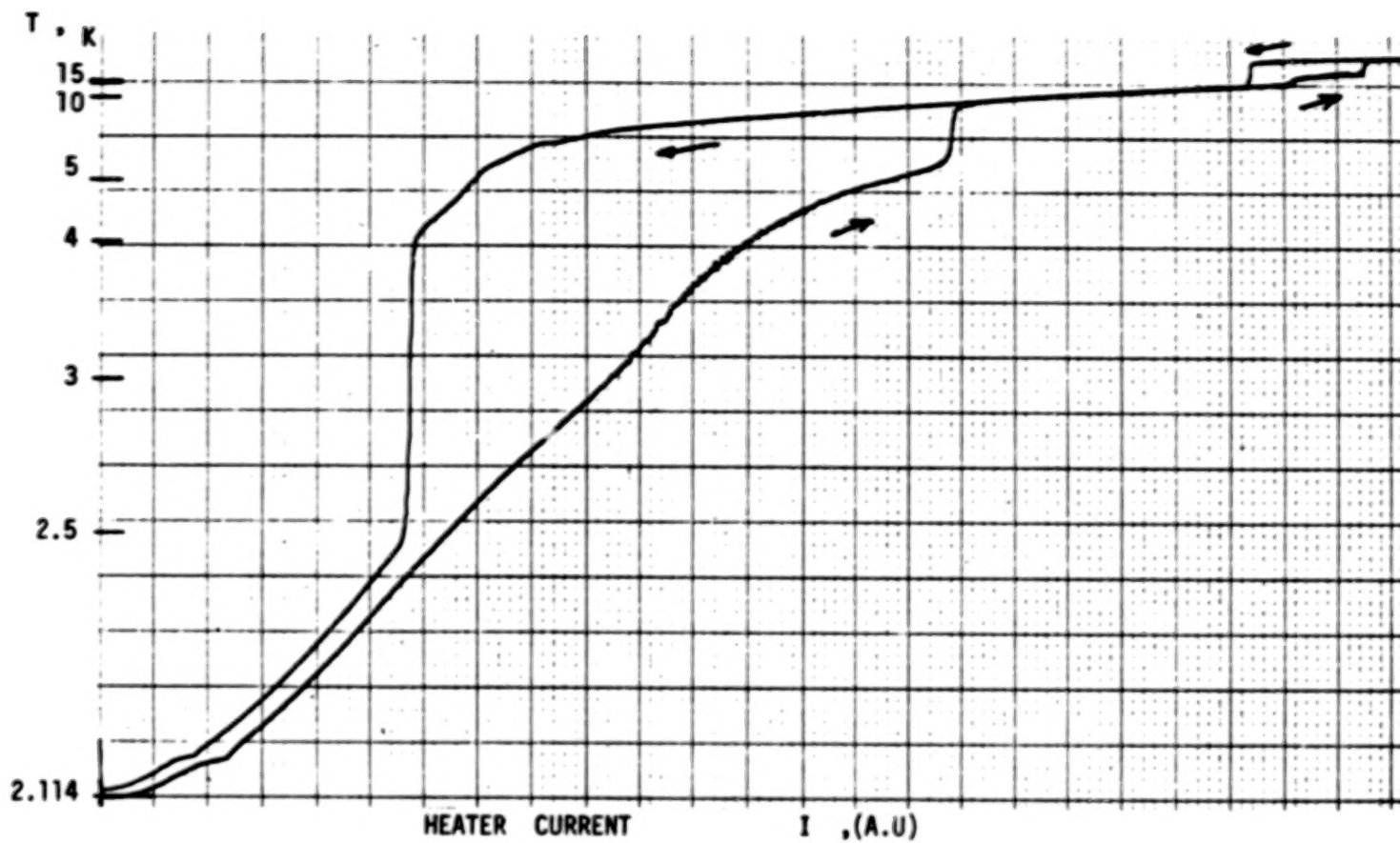


Figure V.5 He II-He I vapor transitions at subcritical pressure (2.12 bar), sample IS-1

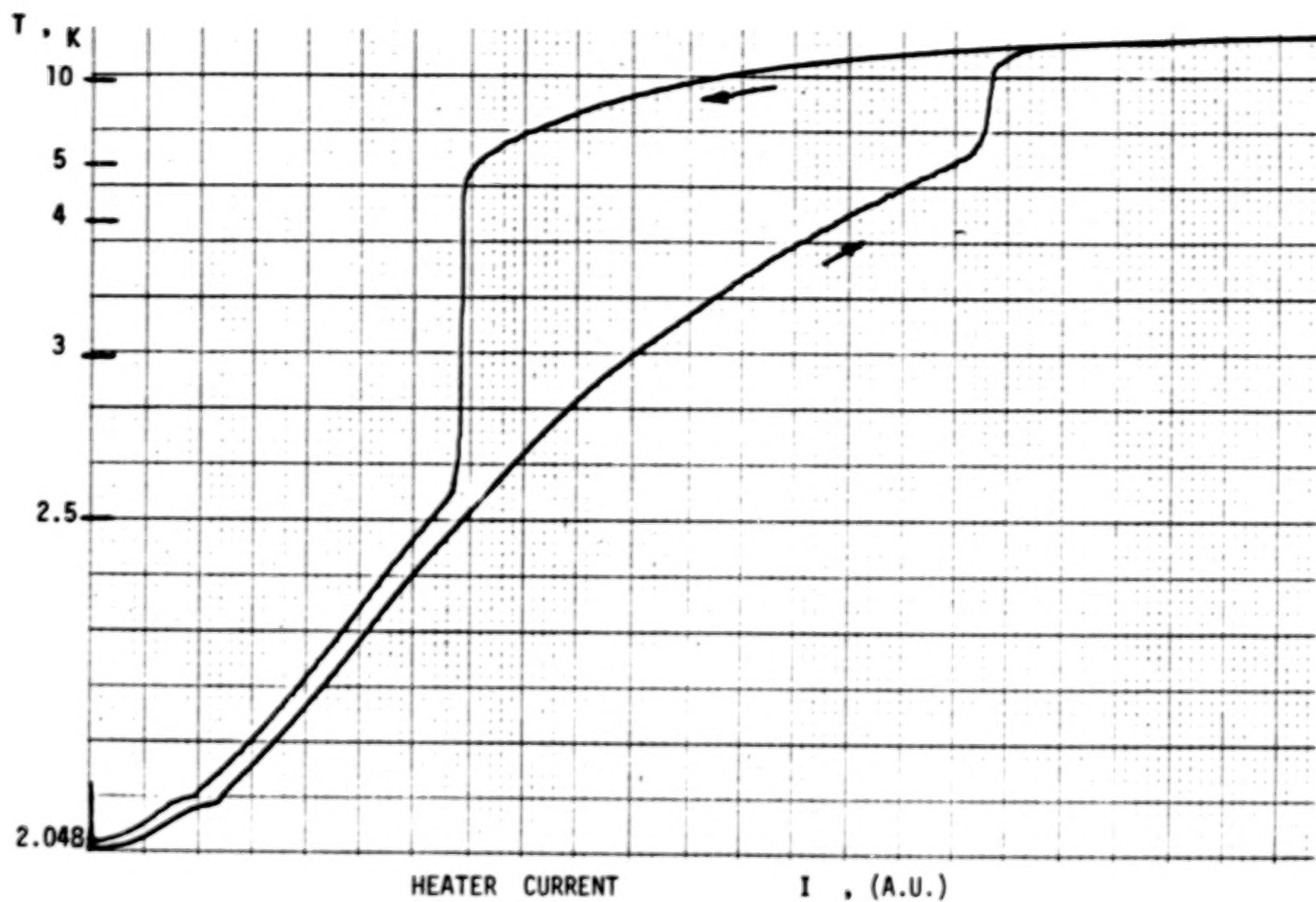


Figure V.6 He II-He I transition at supercritical pressure (7.8 bar), sample IS-1



Limiting heat flux densities at the cessation of single-phase (bulk) He II are shown as  $q_{\lambda} (T, P)$  in Figure V.7. These results have been obtained with the first specimen IS-1A during the first runs above the pressure of saturated liquid He<sup>4</sup>. The data appear to be quite low compared to the runs with near-saturated He II. This result has been in part a consequence of heat exchanger limitations (corrected in subsequent runs). Thus, the data shown represent an operational anomaly in a solenoid system when the heat exchanger is overloaded.

As the pressure is raised, the lambda - temperature decreases. If the thermophysical property variation is not pronounced, the initial asymptotic portion of the function  $q_{\lambda} = q_{\lambda} (T_{\lambda} - T)$  is expected to be similar to the function for near-saturated He II. Accordingly, the data at high P should be somewhat below the data for low P - values. Despite some data scatter, the results confirm a slight reduction of  $q_{\lambda}$  with increasing pressure (at a constant  $(T_{\lambda} - T)$ ).

Other data for pressurized He<sup>4</sup> are discussed in Section V.A.4. Further, we remark that heat transfer coefficients (overall  $\bar{U}$ -values) are considered in the subsequent Section V.A.5.

We turn now to a discussion of the influence of additional coatings on the peak heat flux density  $q_p$ .



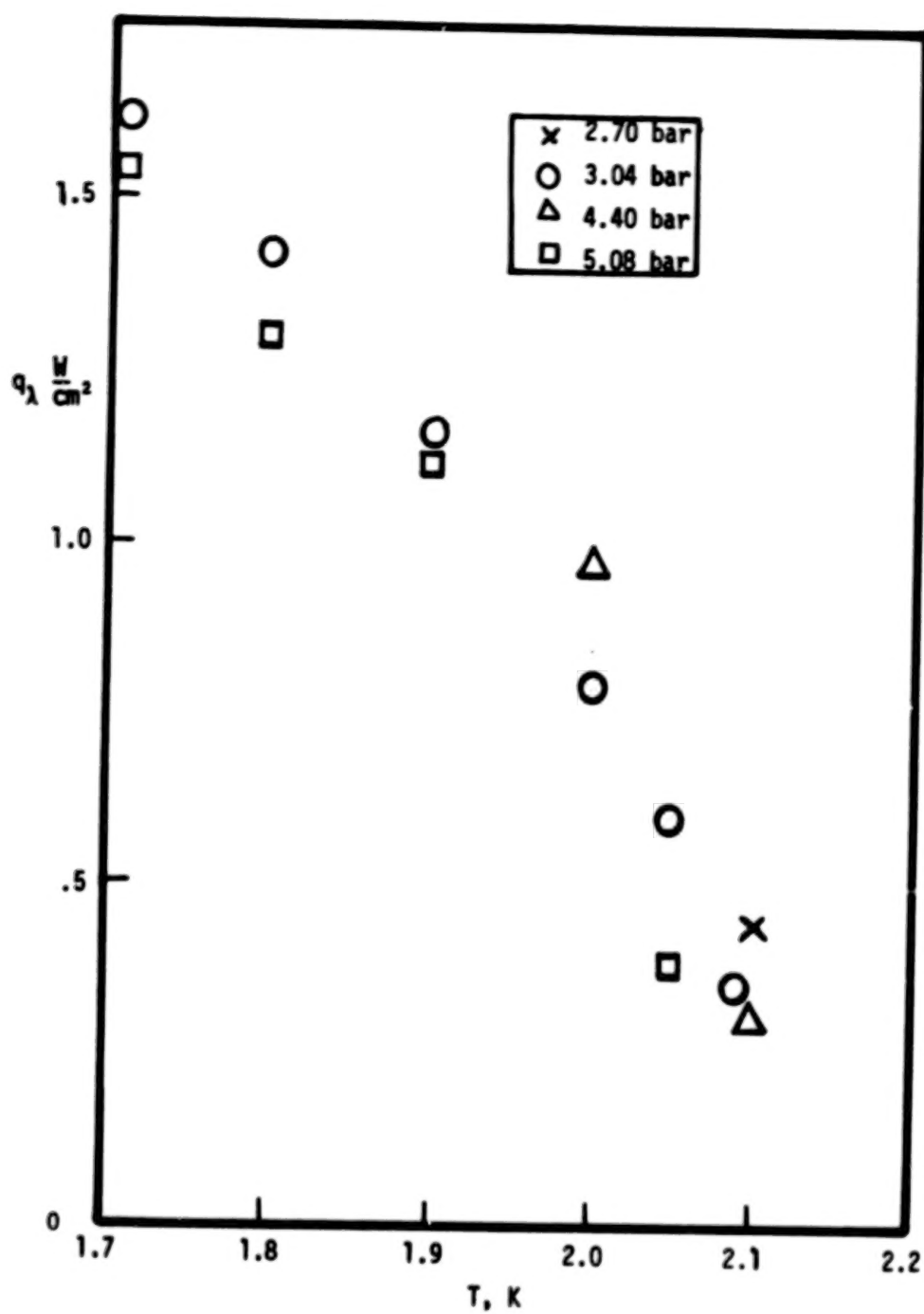
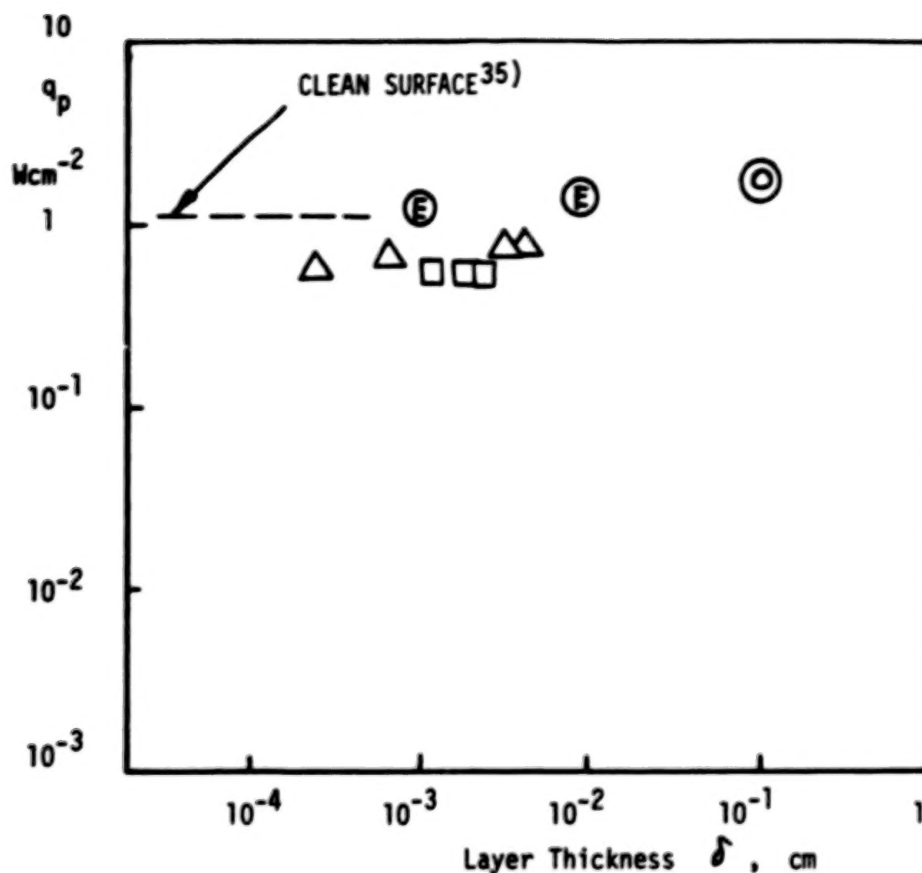


Figure V.7 . Limiting heat flux densities  $q_\lambda$  (T)

### V. A. 3. INFLUENCE OF ADDITIONAL INSULATING COATINGS

It has been desirable to learn about possible effects originating from the application of organic and other coatings. In the past several investigators have been concerned with the increase in  $q_p$  caused by coatings of low thermal conductivity. (This subject has been discussed also in conjunction with nuclear reactor safety work.). More specifically, in the area of superconductor-He I interaction the recent studies of Butler et al. (Reference 34) have determined the change of  $q_p$  for a number of coatings. The results suggest that there is a relatively minor increase in  $q_p$  up to a certain coating thickness  $\delta$ . As  $\delta$  is increased further, no significant change in  $q_p$  seems to exist. Other results (Reference 35) appear to suggest that there may be additional slight changes in  $q_p$  to higher values. However, the data indicate that possibly the switching between an upper  $q_p$ -value and a lower recovery value ( $q_R$ ) may be entirely eliminated. Figure V.8 plots these data which include crude estimates (identified by (E)) of the coating thickness  $\delta$ .

In order to obtain a clear indication of changes, we have coated the specimen IS-1 with a rather thick layer of Dow Corning vacuum grease (silicon lubricant). The layer thickness was about 1 mm. Comparisons of runs with and without grease layer are contained in Figures V.9 and V.10. There are distinct changes in the temperature "seen" by the interior thermometer. In other words, the grease layer constitutes an additional thermal resistance which brings the superconductor closer to the transition temperature  $T_{sn}$ . No thermal switching was observed in these runs. Therefore, the two thermal resistances in series (formvar coating and grease layer) are very effective in lowering the surface temperature of the outer liquid-wetted layer to nucleate boiling temperatures. Obviously for an optimization a thorough knowledge of one single formvar (or other layer) is useful. This implies quantification of the thickness influence. We conclude that no great incentive exists (for most of the present states) to raise  $\delta$ .



**Figure V.8. Peak Heat Flux Density as a Function of Coating Thickness;**

Circles : R.D. Cummings- J.L. Smith <sup>35)</sup>

Triangles: Butler et al. <sup>34)</sup>

Squares: Butler et al. : P.V.A. Enamel layers;

(E) = ESTIMATED

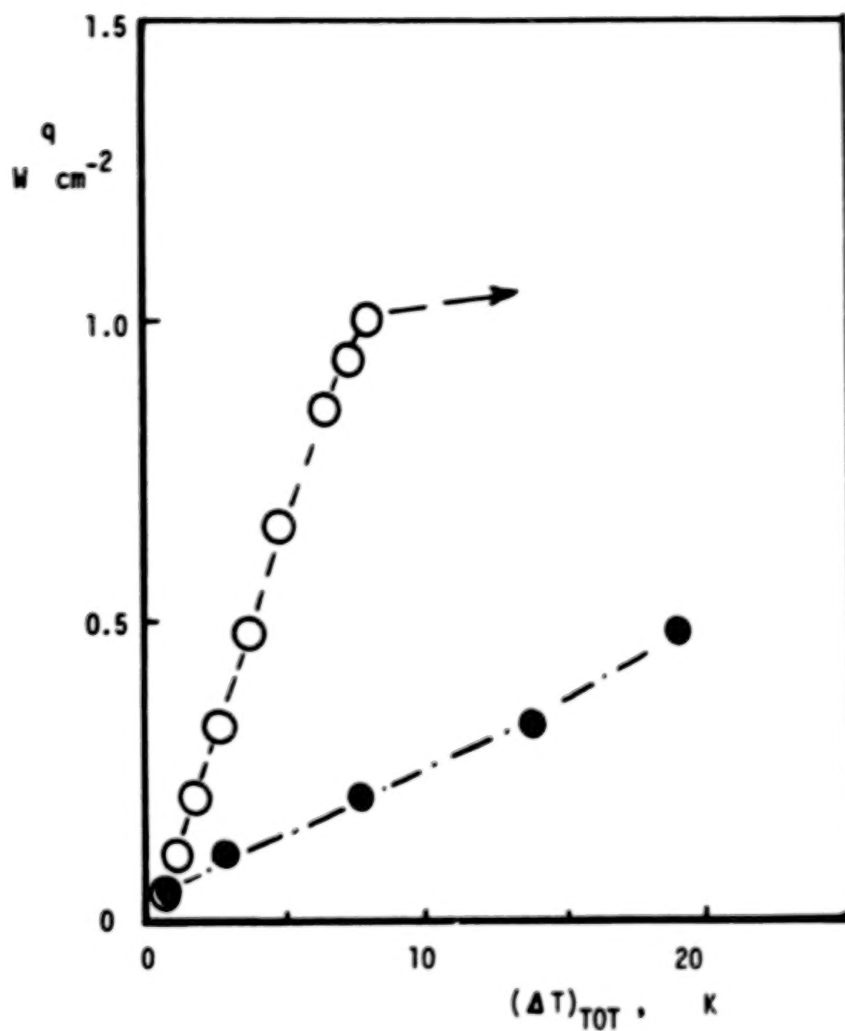


Figure V.9. Heat Flux Density vs. Overall Temperature Difference ( indicated by interior thermometer) at a Bath Temperature  $T = 4.2\ K$  ;  
 Open Circles : Without Grease;  
 Full Circles : With Grease Cover ;  
 (Specimen : IS-1 )

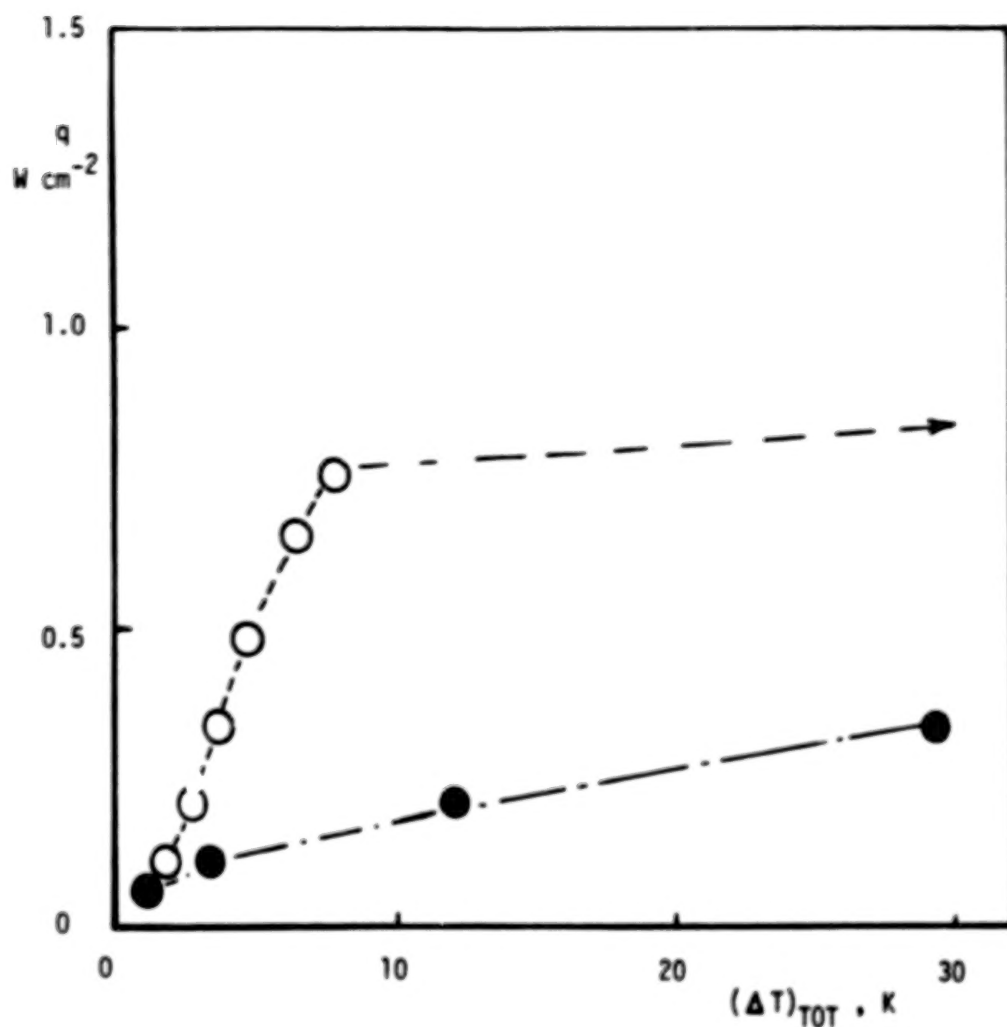


Figure V.10. Heat Flux Density vs. Overall Temperature Difference ( indicated by interior thermometer) at a Bath Temperature  $T = 3.0\ K$  ;

Open Circles : Without Grease Cover ;

Full Circles : With Grease Cover ;

Specimen : IS-1

Further pertinent results have been reported recently (Reference 37) for He I. In these investigations the nature of the heating surface , in particular the roughness was found to have a pronounced influence on the fluid phase transition . In part of the data no clear "thermal switching", i.e. no maximum (peak) and minimum (recovery) flux was visible. Instead, the data obtained showed a monotonically increasing function  $q (\Delta T)$ . The metal alloy exhibiting this behavior most distinctly was stainless steel with a quoted roughness of  $0.7 \mu\text{m}$  <sup>37</sup> .

In this context we remark that stainless steel surfaces have been cooled down also from high T in room temperature liquids. When strongly subcooled water was used in nuclear safety work, the cooldown process was characterized by the absence of nucleate boiling (References 38 and 39). Obviously, the nature of the phase transition phenomena in the fluid appears to be quite sensitive to surface details.

#### V. A. 4. QUENCH ONSET DATA

Specimens instrumented for metal resistance thermometry permitted registration of the quench from the superconducting to the normal state. Figure V.11 plots quench onset heat flux densities ( $q_0$ ) versus  $T$ . At the bare sample surface the very large thermal resistance of the formvar layer is absent. Therefore, this specimen displays the well-known increase in surface cooling conditions which result from the replacement of He I by He II at the lambda transition.

In all other cases of formvar-coated specimens however, the thermal resistance of the insulator is large. The latter should produce an even larger  $\Delta T$  at low  $T$ , as  $k(T)$  changes to small values. Despite the formvar layer insulation, the data exhibit a clear change in  $q_0$  at the lambda transition. In other words, the fluid-solid boundary conditions are distinct enough to enforce a "jump" in  $q_0$ . This change however depends considerably upon the choice of the thermodynamic state of the fluid.

At supercritical pressures ( $P > P_c$ ) the He I has a rather small thermal conductivity. As a consequence, also the heat transfer coefficients of the fluid are small. Therefore, lower entropy transfer rates are possible in He<sup>4</sup> above  $P_c$  compared to liquid He I below its critical pressure provided nucleate boiling takes place. An inspection of the data clearly indicates that the transition temperature  $T_{sn}$  may be a most important quantity which controls the quench onset data  $q_0$ . In general  $q_0$  of formvar-insulated specimens is smaller or equal to the peak value  $q_p$ .

The quench onset data are influenced by the fluid conditions in a different way than  $q_p$ . In He II the fluid resistance is quite significantly reduced compared to He<sup>4</sup> at  $P > P_c$ . Therefore, the change in  $q_0$  at  $P > P_c$  is considerably larger than with near-saturated He I. For the latter fluid state the nucleate boiling characteristics seems to affect the function  $q_0(T)$ . All the data appear to be compatible with the condition: As  $T \rightarrow T_{sn}$ ,  $q_0 \rightarrow 0$ .

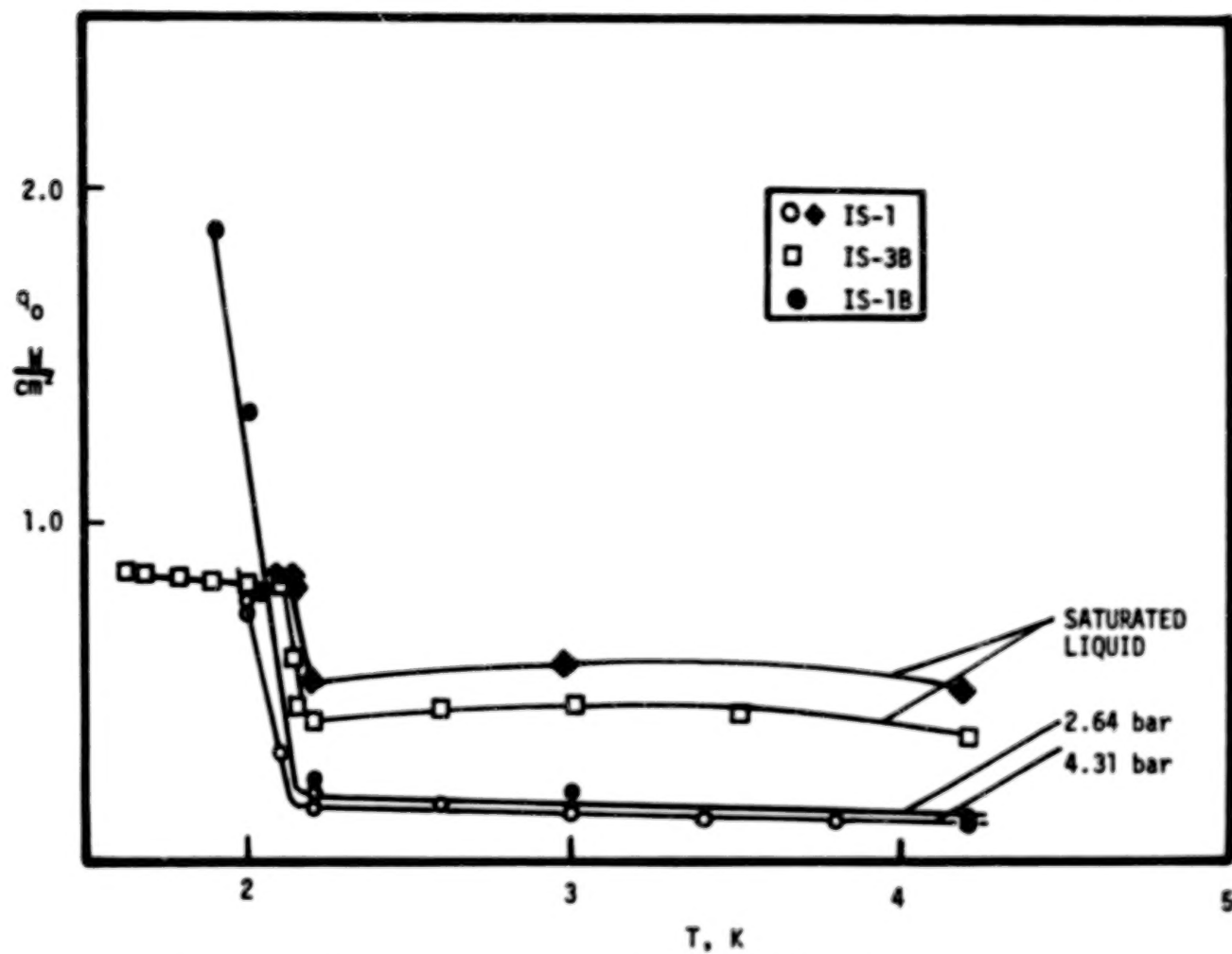


Figure V. 11 Heat flux densities at quench onset conditions



The lambda transition aspects displayed in Figure V.11 are similar to previously reported results, as far as the thermal boundary conditions are concerned. We refer explicitly to Reference 36 which has reported studies of unstabilized NbTi with local flux jumps. This latter aspect is clearly at variance with the present composite. However, the previous work<sup>36</sup> for near-saturated He I and He II shows qualitatively what type of changes may be expected at T.

When the absolute dissipated power is small, the significant change in the thermal boundary condition is the switch from a high Kapitza conductance in He II to a rather low Kapitza conductance in He I. This noticeable change occurs only at rather small  $\Delta T$ -values. Therefore, a minor "jump" in the heat flux density (for the event considered) is observed.

When the absolute dissipated power is large and relatively close to the peak heat flux density ( $q \lesssim q_p$ ), the function  $q_0(T)$  for the event considered shows a pronounced change in the derivative  $dq/dT$  along with a strongly T-dependent part in He II. In most cases the He II portion of the function has a maximum near 1.9 to 2 K, when near-saturated He II is used.

In the present runs the absolute power dissipated at the onset value  $q_0$  is relatively small in most cases. Therefore, the latter possibility is not seen in the majority of the runs. There are some special aspect of stability design considerations for the sizing of formvar and Cu coatings. These will be discussed subsequently. At this point we remark briefly that the quench characteristics indicated qualitative changes for the single specimens used. In He I at high  $q_p$  a gradual change in the resistance of the composite was observed. Around 2.2 K however a relatively sharp transition occurred. This signifies a switch from  $T_{sn}$  - controlled to  $q_p$ -controlled conditions.

## V. A. 5 . HEAT TRANSFER COEFFICIENTS

The emphasis has been placed upon temperature differences not substantially larger than 3 K , and absolute temperatures not significantly in excess of 10 K . The carbon resistance thermometer is quite sensitive in this T- and  $\Delta T$ -range. However, only very small q-values will produce these thermal conditions at the location of the carbon resistance thermometer. In contrast, at the peak heat flux density  $q_p$  , temperatures beyond 20 K were reached readily.

In view of these constraints of the present post-quench scenario studies, we have used phase transition thermometry . Previously fluid phase transition thermometry has been very convenient in the investigations of References 30 to 32. For the present discussion we make use of the transition from the superconducting to the normal state ( $T_{sn} = 8.56$  K , Table III.1)

Figure V.12 plots heat transfer coefficients  $\bar{U}$  at quench onset versus pressure P for various fluid conditions. Most of the data of this graph are of the order of magnitude  $0.1 \text{ W cm}^{-2} \text{ K}^{-1}$  . This relatively small order is a consequence of several thermal resistances in series. We have the following contributions to the overall  $\Delta T$  : A fluid boundary layer resistance in He I ,(replaced by the solid-liquid Kapitza resistance in He II), the thermal resistance of the formvar insulation , the Kapitza resistance between formvar and Cu, a thermal resistance of Cu up to the filament which is in a state of quench initiation.

Between the critical pressure and the lambda temperature of saturated liquid He I (  $T_{\lambda, \text{sat}} = 2.172$  K ,  $P_{\lambda, \text{sat}} = 0.050$  bar) we find in Figure V .12 two data sets for near-saturated liquid . Both show a rather weak influence of the saturated liquid pressure (and T respectively) on  $\bar{U}$  . This behavior is viewed as the result of two dominant contributing factors . First, the nucleate boiling process is

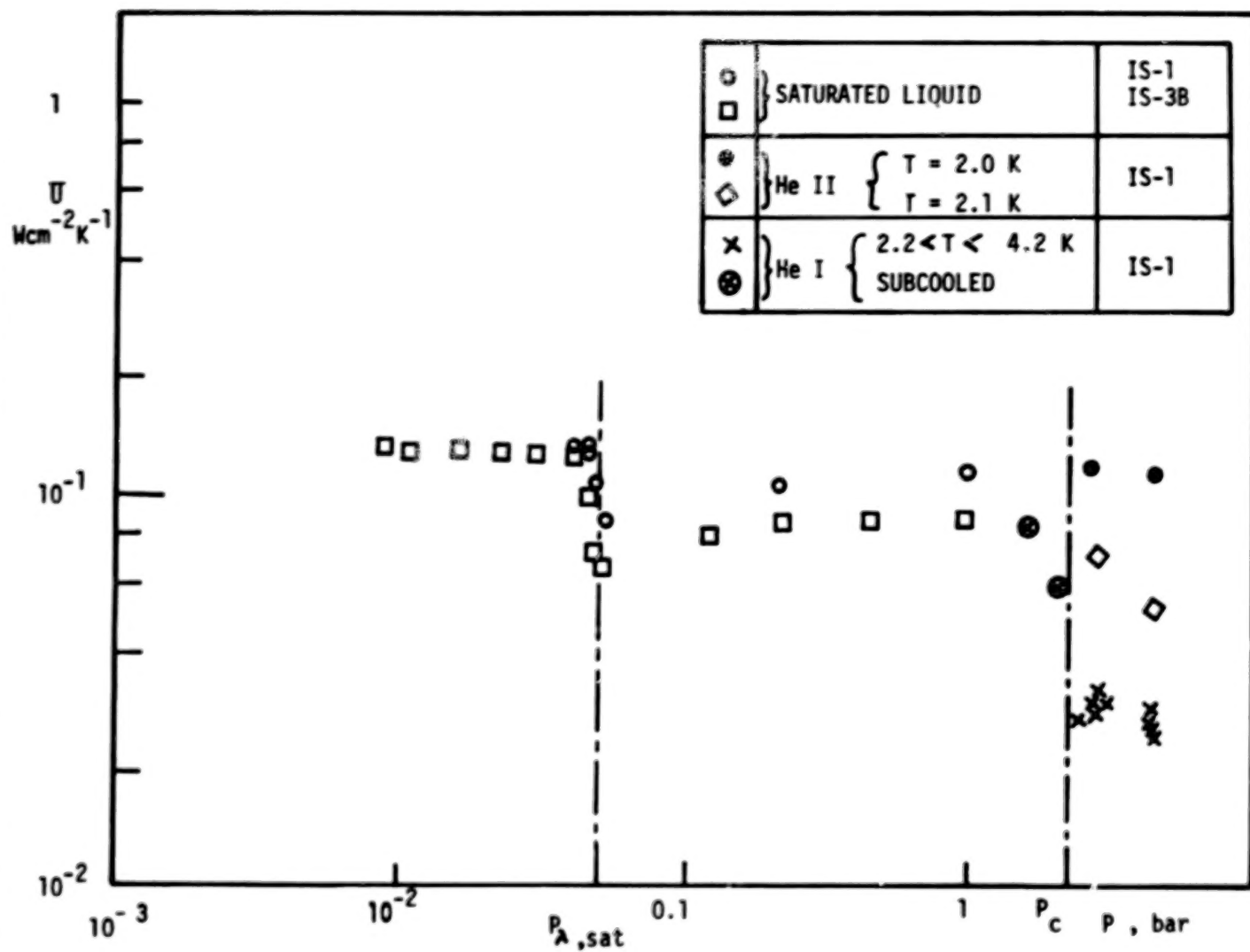


Figure V.12 . Overall heat transfer coefficients of single specimens

characterized by a  $\Delta T$  which increases, as  $P$  is lowered. If all other quantities would be kept constant (in the nucleate boiling regime) this effect is expected to increase  $\bar{U}$  as  $P$  is raised. However, the  $\Delta T$  of nucleate boiling, for a given  $P$ , is not changing drastically. As  $P$  is lowered, the difference between  $T_{sn}$  and the bath temperature increases. This second condition permits larger heat flux densities at the onset of the quench. Accordingly,  $\bar{U}$  turns out to be a rather weak function of  $P$ .

At He II temperatures the data for near-saturated liquid show the well-known increase in  $\bar{U}$  at the lambda transition.  $\bar{U}$  appears to be unaffected by the pressure of the system. The significant change in the series resistance network at the lambda point is the replacement of the classical thermohydrodynamic boundary layer ("boiling layer") by the Kapitza resistance. More accurately, the entire thermal boundary resistance in at solid-He II interfacial domains may be regarded as the sum of a contact resistance and a He II boundary layer resistance. The latter is quite small as the boundary layer is quite thin. It has importance however for the  $q_p$ -values discussed above.

At pressure above the thermodynamic critical pressure ( $P > P_c$ ) the fluid is either subcooled He I, or He I pressurized beyond  $P_c$ . (Sometimes the term "subcooled" has been used also for  $P > P_c$ ; In this case the supercritical fluid is subcooled with respect to the transposed critical curve). The lowest overall heat transfer coefficients are found with subcooled He I for the present single specimens. In He II,  $\bar{U}$  turns out to be a monotonically increasing function of  $(T_\lambda - T)$ , as indicated by data for the two bath temperatures 2.1 K and 2.0 K. Below 2 K, the entropy of He II decreases rapidly to smaller and smaller values. Thus, despite a large  $(p_s/p)$ -value there is no continued rise of  $\bar{U}$ . Therefore, the range below 2 K is not very attractive.

68 A comparison of data below the lambda pressure and results above the thermodynamic critical pressure shows nearly the same  $\bar{U}$ -values

when the temperature is at 2 K . These  $\bar{U}$ -values are quite high. On the other hand the lowest coefficients are found in He I at  $P > P_c$  . Concerning some details of the T-influence in this range we refer to the previous Figure V.11. The dominant factor in the pressurized He I range at  $P > P_c$  is the low thermal conductivity of the fluid. This in turn tends to keep the heat transfer rates down. Accordingly, any operation without supporting forced flow does not appear to be attractive from the post-quench point of view adopted for the stabilizer design approach.

When subcooled He I below  $P_c$  is introduced there appears to be a good chance of recovering high  $\bar{U}$ -values . As all of the present data are for single specimens we refrain from further comments. In magnet channels other factors may have to be considered. The related conductor bundle data will be discussed in Section V.C.

The present  $\bar{U}$ -data are listed in Table V.2.

TABLE V.2  
OVERALL HEAT TRANSFER COEFFICIENT  
Specimen IS-1

$T_b$ , K	P, bar	$\bar{U}$ , W cm <sup>-2</sup> K <sup>-1</sup>
4.20	1.64	$8.45 \times 10^{-2}$
4.20	2.05	$5.81 \times 10^{-2}$
4.20	2.31	$2.68 \times 10^{-2}$
4.20	2.64	$2.98 \times 10^{-2}$
3.79	2.70	$3.12 \times 10^{-2}$
3.40	2.70	$3.37 \times 10^{-2}$
3.00	2.70	$2.75 \times 10^{-2}$
2.60	2.70	$2.73 \times 10^{-2}$
2.20	2.70	$2.80 \times 10^{-2}$
2.10	2.70	$6.96 \times 10^{-2}$
1.99	2.70	$1.15 \times 10^{-1}$
1.90	2.70	$1.24 \times 10^{-1}$
4.20	2.98	$2.98 \times 10^{-2}$
4.20	4.31	$2.48 \times 10^{-2}$
4.20	4.40	$2.50 \times 10^{-2}$
3.80	4.40	$2.54 \times 10^{-2}$
3.40	4.40	$2.44 \times 10^{-2}$
3.00	4.40	$2.55 \times 10^{-2}$
2.60	4.40	$2.57 \times 10^{-2}$
2.20	4.40	$2.72 \times 10^{-2}$
2.10	4.40	$4.97 \times 10^{-1}$
2.00	4.40	$1.19 \times 10^{-1}$
2.00	4.40	$1.12 \times 10^{-1}$

OVERALL HEAT TRANSFER COEFFICIENT

Specimen IS-3B

SATURATED LIQUID

$T_b, K$	$\bar{U}, W cm^{-2} K^{-1}$
4.20	$8.25 \times 10^{-2}$
3.50	$8.50 \times 10^{-2}$
3.00	$8.27 \times 10^{-2}$
2.60	$7.55 \times 10^{-2}$
2.19	$6.43 \times 10^{-2}$
2.17	$7.00 \times 10^{-2}$
2.15	$9.36 \times 10^{-2}$
2.10	$1.19 \times 10^{-1}$
2.00	$1.22 \times 10^{-1}$
1.90	$1.24 \times 10^{-1}$
1.80	$1.24 \times 10^{-1}$
1.70	$1.24 \times 10^{-1}$
1.65	$1.23 \times 10^{-1}$

Specimen IS-1

$T_b, K$	$q_o, W cm^{-2}$	$\bar{U}, W cm^{-2} K^{-1}$
4.20	.51	$1.14 \times 10^{-1}$
3.00	.58	$1.05 \times 10^{-1}$
2.20	.53	$8.39 \times 10^{-2}$
2.15	.83	$1.29 \times 10^{-1}$
2.13	.83	$1.29 \times 10^{-1}$
2.16	.81	$1.27 \times 10^{-1}$
2.17	.57	$8.87 \times 10^{-2}$
2.17	.74	$1.15 \times 10^{-1}$
2.16	.80	$1.25 \times 10^{-1}$
2.10	.83	$1.28 \times 10^{-1}$

## V. B. HEAT CAPACITY EFFECTS

The heat capacity is a quantity of great concern for transient operation. As the runs were conducted with emphasis upon post-quench scenarios during slow quasi-steady conditions, some open questions arise for low  $q$ -values. The overriding temperature drop results from the application of thermal ( and electrical ) insulators ,e.g. formvar. In addition, the initial boundary layer in the fluid is a factor . Even when He II is used, a very thin "miniaturized" boundary layer exists at relatively high  $q$ . Therefore, temperature profile development appears to be an interesting issue. We turn first to the thermal insulator .

In the early literature the heat capacity has been studied only occasionally (e.g. vacuum grease Apiezon N , Reference 40 ). The continuing efforts in the area of cryo-property studies have produced more and more information on epoxy systems (Reference 41 ). Thermal conductivity and heat capacity are connected by the kinetic equation

$$k = (1/3) \rho c_p \langle v \rangle \ell \quad (V.16)$$

(  $\langle v \rangle$  = mean speed of entropy carrier system ,  $\rho c_p$  specific heat per unit volume ,  $\ell$  mean free path ). The thermal diffusivity will decrease for small mean free paths and small carrier velocities.

$$\alpha = k / (\rho c_p) = (1/3) \langle v \rangle \ell \quad (V.17)$$

For instance, the order of magnitude of  $\alpha$  of resins (reported in Reference 41 ) increases as  $T$  is lowered from 20 K to 4 K . This change occurs in the  $\alpha$ -range from  $10^{-2}$  to  $10^{-1}$   $\text{cm}^2/\text{sec}$ . Taking the smallest value of an organic layer of thickness  $10^{-3}$  cm , we note that the time required to obtain thermal penetration is of the order  $10^{-4}$  s. This time is negligible for the present runs.

The thermal diffusivity of the He I is quite small, of the order



$10^{-3} \text{ cm}^2/\text{s}$  . As the solid is heated , the temperature penetrates into a fluid layer of thickness  $10^{-1} \text{ cm}$  in a time interval of the order 10 s. However, as long as nucleate boiling has not occurred yet, the transient heat diffusion may take more time . This is true in particular when the liquid - vapor phase transition is absent at pressures above  $P_c$  .

The previous Figure V. 3 indicates some differences between recorder traces for  $dq > 0$  and  $dq < 0$  at low  $q$ -values. Thus, the transient effects cannot be neglected for small incipient dissipation . At the post-quench scenario of the present heater simulation experiments however, boundary layers or boiling layers appeared to be established quite well.

The Kapitza resistance between a solid and liquid He II is a complicated function involving solid surface conditions and thermal excitations in the liquid He II. The entropy carrier system of the latter is predominantly a roton system which has to adjust to the wall-adjacent phonon system. Accordingly, in the T-range of the present studies (in He II) so far only semi-empirical methods have predicted data trends. A comparison between the formvar-coated sample and the uncoated conductor is not straightforward, due to the presence of several thermal resistances .

As to the Kapitza resistance between the formvar and copper, we refer to the previous comments (Section V.A.1 ).

## V. C. Conductor Assembly Results

Dual specimen runs did not show any drastic departures from data obtained for single specimens. The peak heat flux densities were above  $q_p$  values for saturated liquid. One factor of influence is most likely the effective area available for entropy removal. (A large thermal resistance was either caused by the series connection of two formvar layers, or two formvar layers and a G 10 spacer); This point has been discussed in Sec. V.A.1).

Data of the conductor assembly (bundle of 9 conductors) showed quench heater simulation function quite similar to the results for single specimens. As there were two adjacent conductor sections instrumented with thermometers however, the state of the fluid in the channels of the bundle could be observed in some detail. An example is Figure V.13.

The spacers had a horizontal orientation in the runs of Fig.V.13. Therefore the entropy flow direction from the central heater was within a horizontal plane initially. Up to the quench onset the temperature of the heater sample was deduced from its carbon thermometer signal. Above 20 K the temperature of the central conductor was evaluated from Cu-resistance thermometry. Only a weak film boiling transition (and related hysteresis) was indicated by the thermometer. For an interpretation it is noted that the formvar insulation separates the thermometer quite effectively from the fluid. On the other hand, the adjacent thermometer samples are much closer to adiabatic conditions. Therefore, they sense the state of the fluid readily. As we have He I near saturation, the sensor LB shows temperatures beyond  $T_{sn}$ , and a film boiling hysteresis loop of relatively large width. This indicates that there is some thermal conduction from the central heater specimen (CB) to the adjacent thermometer specimen (LB). The upper thermometer (UB) however, is not in solid contact with the heater sample. We see that the temperature of the sensor is relatively close to the usually observed nucleate boiling temperature of a bare solid. The film boiling hysteresis loop is rather narrow. Thus, the film boiling state of the "lower" heated section is not spread out over the entire duct.

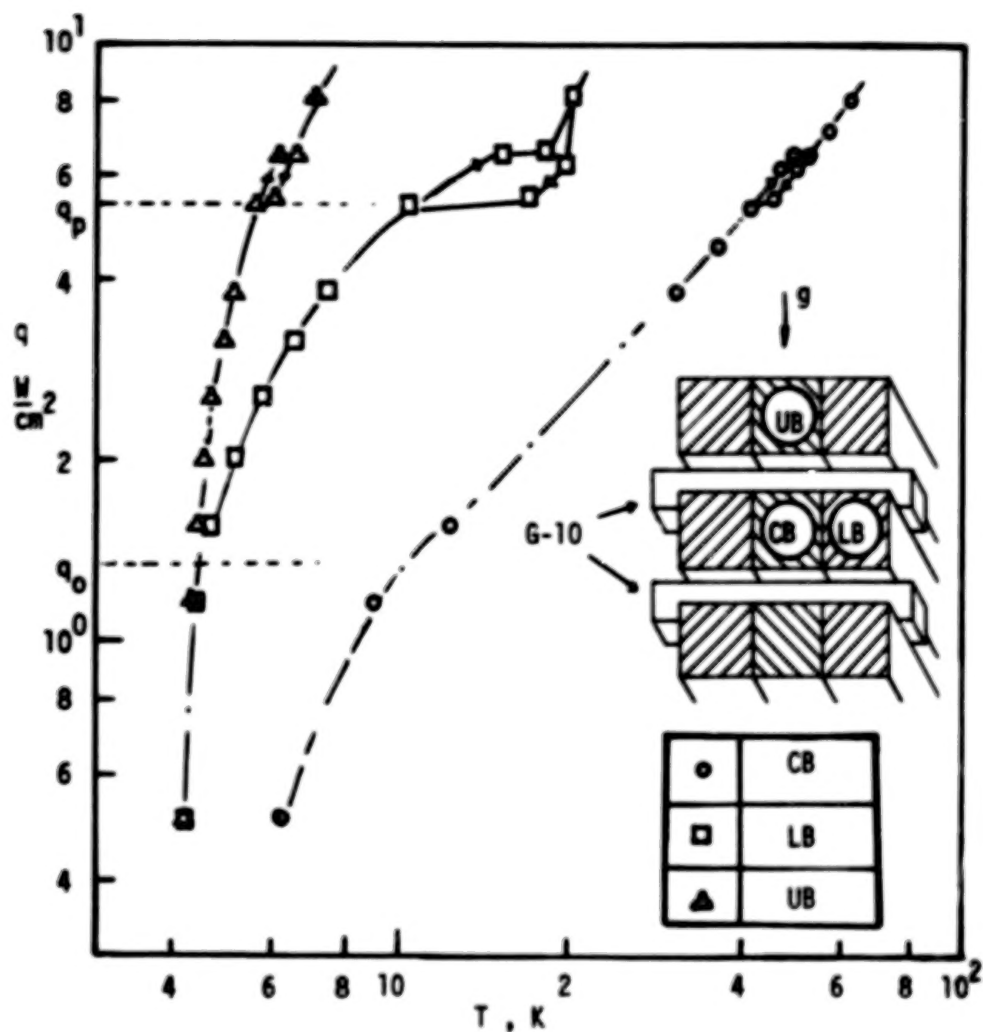


Figure V.13 . Heat flux density of conductor bundle  
(He I , 4.2 K )

For the same He I state (near-saturated liquid at 4.2 K ) the bundle with vertical spacer orientation indicated again a weak hysteresis loop at high T during the transition from nucleate to film boiling. Phenomena similar to Figure V.13 were indicated by the thermometer specimens near the heater. In other saturated He I studies it has been found (Reference 43 ) that the most efficient heat removal occurs when the flow resistance opposing vapor removal is least. (For a horizontal surface this is the case when the vapor flow is up at standard gravitational acceleration). The present results are interpreted ( in part) as evidence for an "easy" vapor removal in the vertical direction.

In superfluid liquid He<sup>4</sup> the He II boundary layer is very thin, i.e. much thinner than the G 10 spacer thickness) . Therefore, the thermometer sample opposite to the heater sample should not be affected drastically by prequench heating of the dissipative sample. Indeed, the thermometer records appear to be consistent with this expectation. The film boiling transition of the heater sample does have some effect upon the opposite thermometer sample . It appeared to be qualitatively similar to Fig. V.13. However the magnitude of the temperature excursion was reduced (compared to Figure V.13). This situation is reflected also in the overall heat transfer coefficients of the bundle (Figure V.14).

Figure V.14 plots  $\bar{U}$  versus P . As the exact surface area for heat removal is not known , a nominal area of the central heater sample exposed to liquid was inserted for  $\bar{U}$ -calculations. The real surface area is larger. Therefore the  $\bar{U}$ -values are higher than the previous data for single specimens (Figure V.12) . One aspect of bundle phenomena departs significantly from results for single specimens. The He II data are considerably larger than the values for He I at 4.2 K . Further, the lowering of  $\bar{U}$  at about 2.2 K ( above the lambda transition) is more drastic than for the single specimens.

The use of He II has been contemplated in many conceptual design studies for NbTi. However the advantage gained by a higher critical current density and a larger critical magnetic field has to be assessed

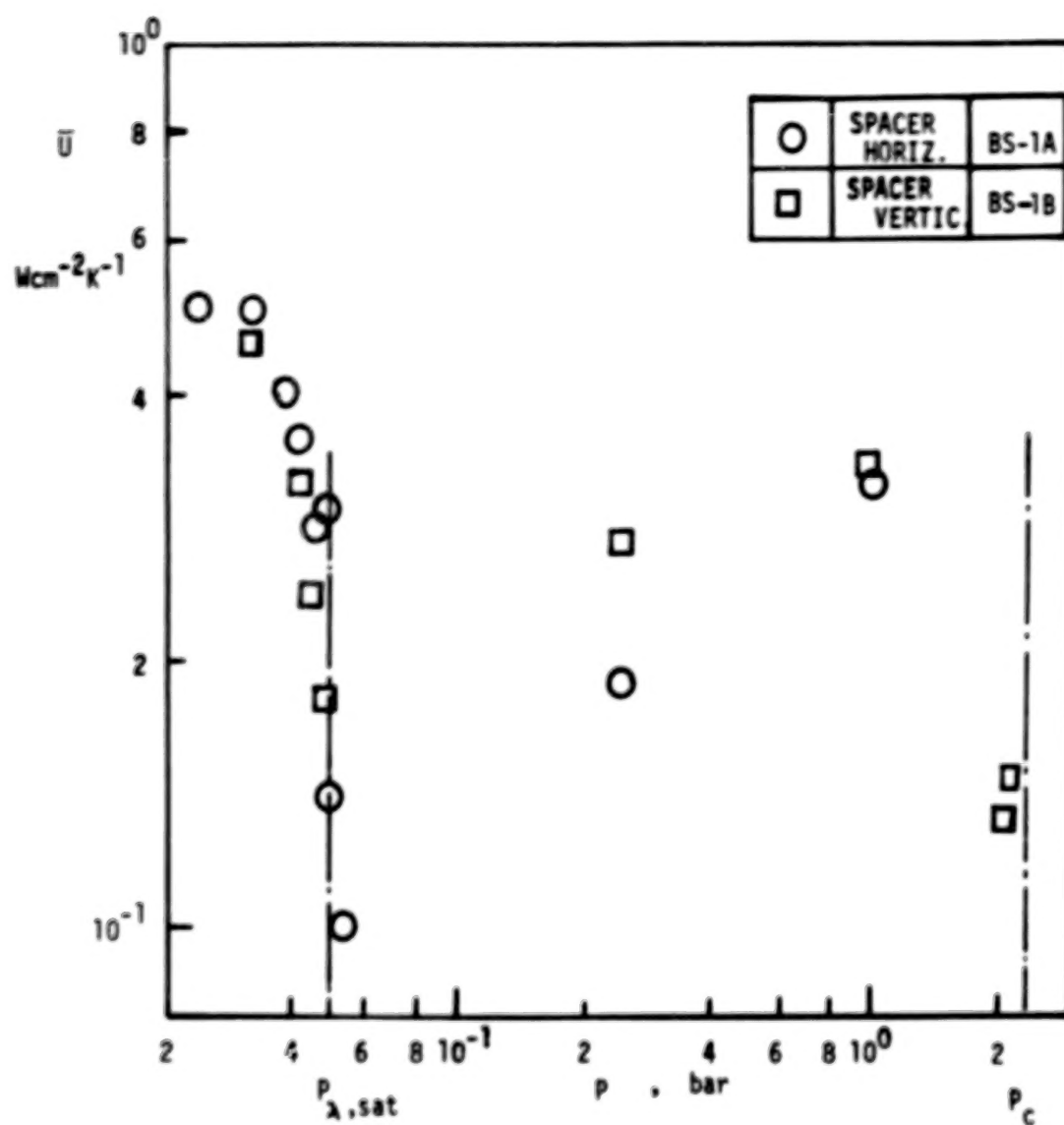


Figure V.14 . Overall heat transfer coefficient of conductor bundle

not only from the point of view of post-quench safety phenomena, but also from the refrigeration requirements aspects. In the area of post-quench conditions the entire range of T-excursions is an important point. Though the present discussion so far has focussed on the pre-transition quantities, the post-transition behavior cannot be ignored. For the pressurized He II above  $P_c$  the post-transitions of bare samples studied earlier ( Reference 44) indicate rather small T-excursions of a few K. In the present bundle runs however the temperature rise was above  $T_{sn}$ . One phenomenon not understood entirely was the reversal in behavior (with respect to He I ) when the orientation was changed. In He II the horizontal spacer orientation showed more favorable thermal conditions than the vertical arrangement. In He I the opposite was true.

Concerning refrigeration there has been considerable research in the area of forced convection of He II. Many investigators have shown that near-isothermal He II will undergo a transition to classical Newtonian behavior at rather small Reynolds numbers. Furthermore, studies of the Leiden group ( e.g. Reference 45 and many related papers) have established a significant change in the Gorter-Mellink flow when a piston displaced the liquid. A recent paper ( Reference 46) has confirmed this modification of He II convection toward a less powerful classical heat transfer mode. However, these latter investigations may be considered simulation studies of piston engines with local acceleration involving the partial derivative of the velocity with respect to time. Thus, all engines (centrifugal pumps , piston compressors etc) show near-classical behavior as the Reynolds numbers of these devices are high. The attractive point of He II operation however is the possibility of thermomechanical pumping with systems which have no moving components. This peculiarity of He II is to be kept in mind when the details of the refrigeration mode for a He II-cooled magnet are designed.

$\bar{U}$ -data are listed in Table V.3.

TABLE V.3  
OVERALL HEAT TRANSFER COEFFICIENTS  
OF CONDUCTOR BUNDLE  
Specimen BS-1A  
(spacers horizontal)

$T_b, K$	$\bar{U}, W\ cm^{-2}\ K^{-1}$
4.20	.32
2.99	-
3.00	.19
2.20	.10
2.16	.14
2.15	.30
2.13	.28
2.11	.36
2.07	.41
2.05	.50
1.90	.50

Specimen BS-1B  
(spacers vertical)

4.20	.33
3.00	.27
2.16	.18
2.13	.24
2.10	.32
2.00	.46

## V . D. FRICTION RESULTS

The friction coefficients ( $\mu_F$ ) have been determined calorimetrically from the power dissipation occurring at contact locations between formvar-insulated conductors. During these measurements the temperature difference between the thermometers (one on the solid, another one in the liquid of the test chamber) and the outer bath was  $\Delta T \ll T$ . Therefore,  $\Delta T$  could be deduced from the slope  $\beta_g = d \log R / d \log P$  of the resistance pressure function  $R(P)$ . This calibration function of the carbon thermometers is nearly a linear function in logarithmic coordinates (i.e.  $\beta_g \approx \text{const.}$ ) in the He II range of  $T$ . Subsequently the heat flow meter function (described in Section IV) allowed determination of the power dissipation  $\dot{Q} = \dot{W}$ . The work per unit time ( $\dot{W}$ ) is the product of the friction force  $\mu_F F_g$  and the tangential velocity ( $\Omega \cdot \bar{D}/2$ ) of the upper rotating ring of formvar-coated conductor. Therefore the friction factor may be written as

$$\mu_F = \frac{\dot{Q}}{(\bar{D}/2) \Omega F_g} \quad (\text{V.18})$$

( $\Omega$  angular speed,  $\bar{D}$  mean diameter of upper rotating ring,  $F_g$  weight).

Figure V. 15 plots the friction factor obtained during quasi-steady slow motion (mostly at 16 RPM) versus the temperature. A lower bound to the data has been evaluated from a special heat leak test of the heat flow meter. The  $\mu_F$ -data incorporate a relatively large scatter. Thus, it appears to be quite difficult to discern a significant influence of  $T$ . The absolute values of  $\mu_F$  appear to be quite compatible with other low temperature friction factors. Reference 47 may be consulted for a comparison of friction data.

In the superfluid liquid He II there is most likely no lack of liquid wetting of the conductors in contact with each other. At contact locations the low viscosity of the normal fluid is expected to be of no essential assistance, as far as a hydrodynamic lubrication effect is concerned. On the other hand, a liquid He II film is able to come close to contact domains.



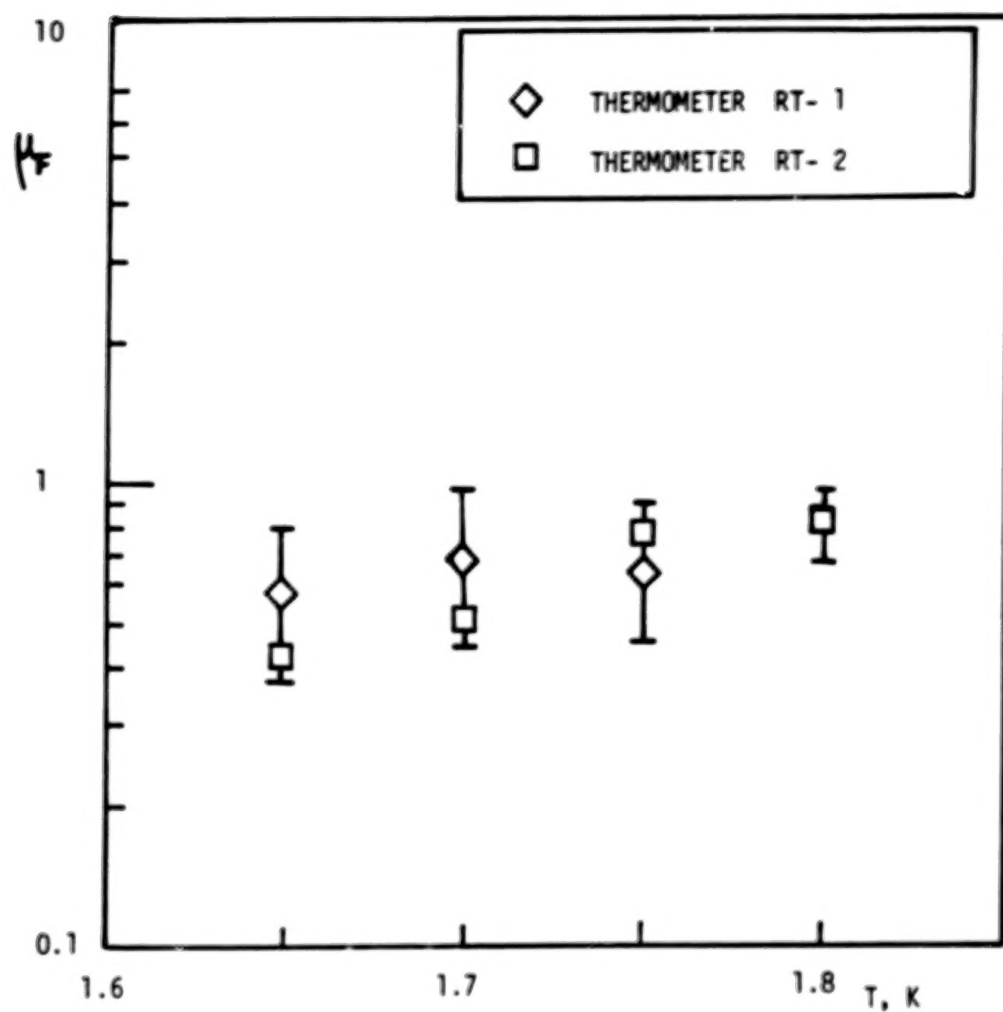


Figure V.15. Friction factor versus temperature  
 ( RT-1 Thermometer attached to composite super-conductor;  
 RT-2 Thermometer in liquid adjacent to solid )

As the latter are dissipative, thermomechanical flow of superfluid toward the hot spots is expected to occur. As the axial thermal conductivity of the composite however is quite large compared to the radial value, it is expected that the  $\Delta T$  at the dissipative location may not be as high as the adiabatic limiting value for  $\Delta T$ .

## VI. CONCLUSIONS

The order of magnitude of the friction factor data obtained shows that some care is necessary during design and construction of "jelly roll" magnet assemblies. Any displacement of winding sections relative to each other during magnetic pressure changes will favor a local quench. The final outcome (quench or no quench) will depend on the region of composite affected by the dissipation of energy. Without a knowledge of these details quantitative prediction is difficult, however the magnitude of the friction factor is sufficiently large to induce attention to this problem.

The major portion of this work was devoted to the magnet composite in a post-quench scenario. To place the conclusions into appropriate perspective a clear separation of two issues is useful. One point is the type II superconductor itself. Its pinning properties, related filament sizing and twist procedures, and manufacturing conditions should be recognized as a set of specifications remote (at first view) from the second issue. The latter is the thermal and thermohydrodynamic choice of coolant conditions and related safety sizing of stabilizer and insulator. As far as the first issue is concerned it has been assumed that satisfactory conditions have been met. A few checks of type II quantities during the initial phase of the present runs indicated that indeed the type II behavior is satisfactory.

The second issue is the post-quench scenario. Any choice of criteria for the sizing of the normal metal stabilizer and the insulator thickness, the coolant channel width and orientation may be based on a wide range of possible design choices. It is noted that the majority of coolant choices considered for  $\text{He}^4$ -cooled magnets involves at least one fluid phase transition. The widespread uncertainty concerning quantitative information in this area is related to the fact that two phase transitions (one in the solid state, another one in the fluid state) may influence each other. Once the type II has seen quench initiation, it is the possibility of a fluid phase transition which modifies the solid-coolant interaction

to a complex phase transition scenario . By choosing a heater simulation technique during quasi-steady heat flow, we have restricted the total set of possibilities to a smaller subset (of quasi-steady conditions). The latter may form the basis for design procedures for the sizing of normal metal stabilizers and insulating layers.

From the results obtained during the present runs we conclude that there are two safety regimes for the present composite. One safety case is associated with a  $T_{sn}$  -criterion. It is characterized by a thick formvar layer which brings the composite temperature readily to  $T_{sn}$  when  $d q > 0$  . The other safety case is characterized by thin formvar layer. Now the power density at the surface (=peak heat flux density) is the crucial factor. This second criterion brings about a rapid increase in  $T$  of the solid in most cases which involve film boiling transitions. A switch from one case to the other situation was possible by varying the thermodynamic state of the fluid.

To quantify these conditions we equate the two heat flux densities associated with both safety criteria for an evaluation of the limiting thickness

$$q_p = \bar{k} (T_{sn} - T) / \delta_L \quad (VI.1)$$

Thus, the limiting thickness  $\delta_L$  will be

$$\delta_L = \bar{k} (T_{sn} - T) / q_p \quad (VI.2)$$

In these two equations  $\bar{k}$  represents the mean value of the entire set of thermal conductances seen by the composite . In the present case the main contribution comes from the formvar layer. Accordingly, the related (mean)  $k$ -value has been inserted for a numerical evaluation (Figure VI.1).

Figure VI.1 plots  $\delta_L$  versus  $T$  . Further, the existing formvar thickness is denoted as  $\delta_{fv}$  . At 4.2 K the present formvar layer is "thick" with respect to the limiting value . At 2.2 K however, this is

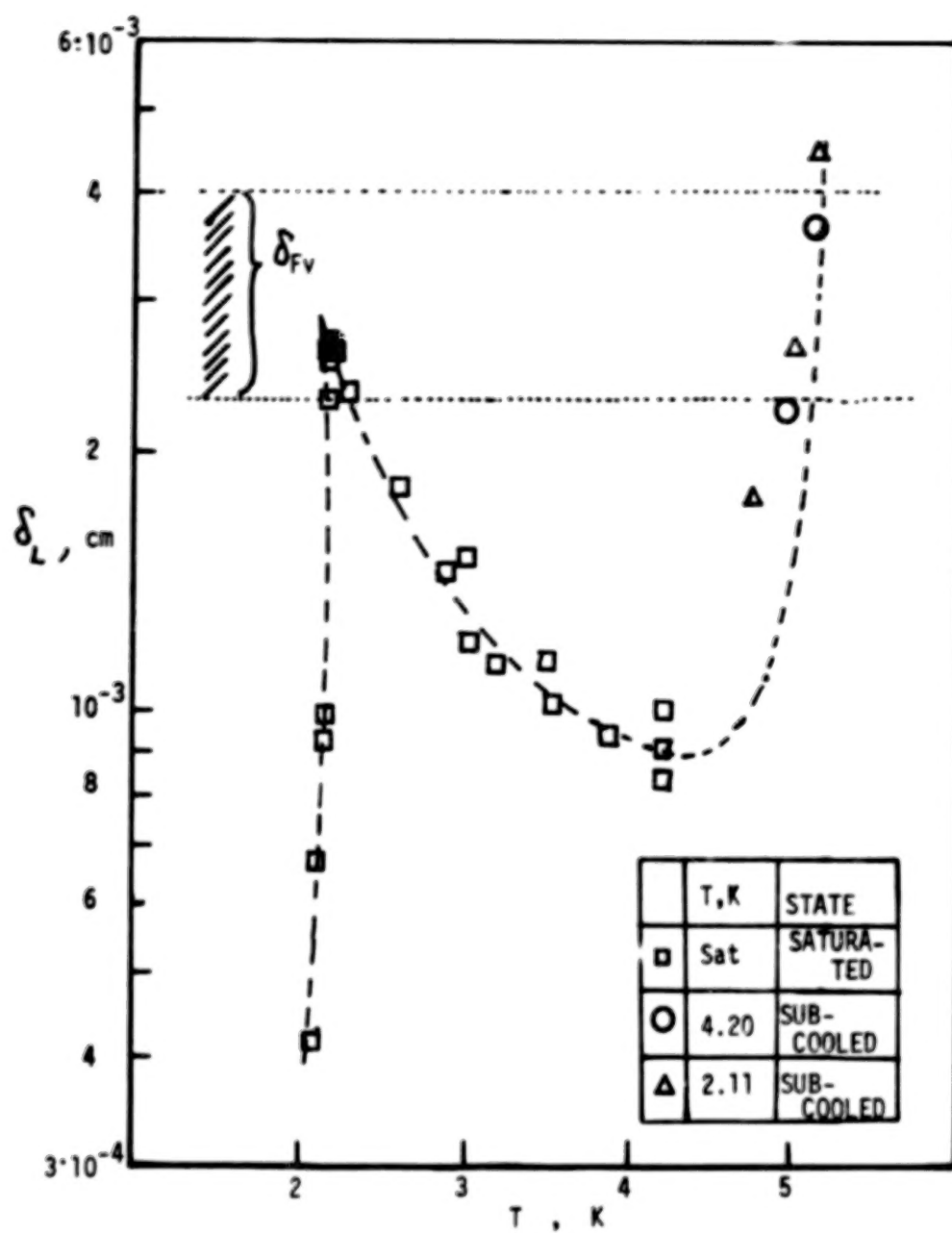


Figure VI. 1 . Limiting thickness versus T

no longer the case. At this temperature and at the lambda transition the existing  $\delta_{FV}$  starts to become thin with respect to the limiting value. In He II at  $T$  below the lambda transition the existing  $\delta_{FV}$  is again thick with respect to the limiting  $\delta_L$ . Figure VI.1 has been calculated on the basis of data for single specimens. The X-Y-plotter records observed during the quenches were indeed consistent with this  $\delta_L$ -discussion.

With the composite bundle different results were obtained. Though the exact heat leak and the area carrying heat flow was not known well, the records of the quench characteristics provided information about  $q_p$ . Over most of the He I range from the normal boiling point to  $T_\lambda$ , rather sharp transitions were obtained except in the vicinity of 4.2. This is interpreted as evidence for reduced  $q_p$ -values. In He II however the enhancement in  $q_p$  was distinct. This indicates that the layer thickness  $\delta_{FV}$  is quite large with respect to the limiting value.

Obviously the designer has the choice of a suitable  $\delta_{FV}$  and another choice of  $A_{cu}$ . There seems to be some incentive to go close to the limiting value  $\delta_L$ . On the other hand, it is desirable to incorporate enough safety into most magnets. Therefore, one may choose to have a safety factor  $> 1$  for the copper stabilizer, and in addition a safety factor  $> 1$  for the formvar layer thickness. In He I the present data indicate that one may reduce the formvar layer thickness below the value  $\delta_{FV}$  of the existing composite.

In pressurized He II similar thickness conditions were found.

# REFERENCES

1. Kantrowitz , A.R. and Stekly, Z.J.J., Appl. Phys. Letters, Vol.6, p. 56 , 1965
2. Stekly, Z.J.J. , J. Appl. Phys. Vol. 37, p. 324, 1966
3. Whetstone, C.N. , Chase, G.G. , Raymond, J.W., Vetrano, J.B., Boom, R.W. , Prodehl, A.G. and Worwetz, H.A., IEEE Trans. on Magnetics , Vol. MAG-2, p. 307 , 1966
4. Hust, J.G. , Cryogenics , Vol. 15, p. 8 , 1975
5. Hulm, J.K. and Blaugher, R.D. , Phys. Rev. Vol. 123,p. 1569, 1961
6. Dubeck, L. and Setty, K.S. , Phys, Letters , Vol. 27A,p. 334, 1968
7. Shapira Y. , and Neuringer,L.J., Phys. Rev. Vol. 140,p. A1638,1965
8. Berlincourt, T.G. and Hake , R.R., Phys. Rev. Vol.131, p. 140,1963
9. Caspi, S. , Chang, Y.W., Lee, J.Y. and Frederking , T.H.K. , Rept. Univ. California, UCLA-ENG-7649, 1976
10. Caspi, S. , Chang. Y.W. , Lee, J.Y. , and Frederking, T.H.K., Rept. Univ. California, UCAL-ENG-76109, 1976
11. Linnet, C., Purdy, V., Chang, Y.W. and Frederking, T.H.K., Rept. Univ. Calif. , 69-62 , Oct 1969
12. Goodling, J.S. and Ireys, R.K., Adv. Cryog. Eng., Vol. 14,159, 1969
13. Schmid , C. , Phys. Rev. Vol. B 15, p.4187, 1977
14. Matsumoto, D.S. , Reynolds, Jr., C.L. and Anderson, A.C. Phys. Rev. Vol. B ,p. , 1977
15. Krafft, G., (transl.) , Rept. KFK-1786 , Karlsruhe Nucl. Res. Center April 1973; STS Inc. June 1975
16. Keesom, W.H. , Saris, B.F. , and Meyer,L., Physica, Vol. 7,p. 817,1940
17. Kapitza , P.L., J. Phys. USSR, Vol. 4 , p. 181 1941
18. Keesom, W.H. , and Duyckaerts, G., Physica Vol. 13, p. 153, 1947
19. Vinen, W.F., Proc. Roy. Soc. (London), Ser. A, Vol. 240,p. 114, 1957
20. Chase, C.E. , Phys. Rev. Vol. 127, p. 361 , 1962
21. Vicentini-Missoni, M.,and Cunsolo, S., Phys. Rev. Vol. 144 , p. 196, 1966
22. Chritchlow,P.R. and Hemstreet, R.A. , J. Appl. Phys. Vol. 40 , p. 2675, 1969
23. Passow,C.H., Aupelt, G., Bergotz,R.,Heneka,A.,Herz,W.,Paetzold,H. Schaphals,L.and Spiegel,M.J., Cryogenics Vol.11,p.143, 1971
24. Linnet, C. and Frederking, T.H.K., Progr. Refrig. Sci. Technology, Vol. I (Proc. 13th I.I.R. Congr.) AVI Publ. Comp. Westport, Conn. 1973, p. 253

25. Stephens, R.B. , Cryogenics , Vol. 15 , p. 420 , 1975
26. McTaggart, J.H. , and Slack, G.A. , Cryogenics , Vol. 9, p. 384, 1969
27. Dahl, A.I. , private communication : Thermal cond.  $k = 3.2 \times 10^{-5}$   
W cm<sup>-1</sup> K<sup>-1</sup> for 4 to 6 mil samples between Cu-surfaces
28. Denner H., Cryogenics Vol. 9 , p. 282 , 1969
29. Frost, W., (Ed.) , "Heat Transfer at Low Temperatures", Plenum Press,  
New York , 1975
30. Haben R.L. , Madsen, R.A. , Leonard, A.C., and Frederking, T.H.K.  
Adv. Cryog. Eng. Vol. 17, p. 323 , 1972
31. Leonard, A.C. and Clermont, M.A., Proc. 4th Int. Cryog. Eng. Conf.  
Eindhoven , May 1972, PIPC. Sci. Technol. Press Ltd.  
London, 1972, p. 301
32. Soloski, S.C. , unpublished data \*)
33. Berenson, P.J., J. Heat Transfer, Vol. 83C, p.351 , 1961
34. Butler, A.P. , James, G.B., Maddock, B.J. and Norris, W.T., Int-  
J. Heat Mass Transfer, Vol. 13, p.105, 1970
35. Cummings, R.D. and Smith, J.L., Liquid Helium Technology , IIR  
Comm. 1, Annexe 1966-5, Proc. Boulder Conf. 1966,p.85
36. Frederking, T.H.K. , and Linnet, C. Adv. Cryog. Eng., Vol. 13,p.80,  
1968
37. Grigoriev, V.A. , Klimenko, V.V., Pavlov, Yu.M., Ametistov, Ye.,V.,  
and Klimenko, A.V., Cryogenics, Vol. 17, p.155, 1977
38. Dhir, V.K. and Purohit, G.P., ASME Paper 77-HT-78, National Heat  
Transfer Conference, Salt Lake City, Utah, Aug.1977
39. Dhir, V.K., private communication
40. Bunting, J.G. Ashworth, T, and Steeple, H. Cryogenics Vol. 9,  
p. 385, 1969
41. Hartwig, G., Adv. Cryog. Eng. Vol. 22, p. 283, 1976
42. Amar , R.C. , Ph. D. thesis , Univ. Calif. Los Angeles, 1974
43. Lyon , D.N. Int. Adv. Cryog. Eng. , Vol.10, p. 371, 1965
44. Caspi, S. , Lee, J.Y., Soloski, S.C. and Frederking, T.H.K.,  
Rept. Univ. California, UCLA-ENG-7713, 1977
45. Van Alphen, W.M. , Vermeer, W., Taconis, K.W. and de Bruyn Ouboter,  
R., Low Temp. Phys. LT-9, Proc. XIth Int. Conf. Low  
Temp. Phys. (Ed. J.G. Daunt et al.), Pt.A, Plenum Press,  
1965,p.323

-----  
\*) Ph. D. thesis expected to be finalized in near future



46. Johnson, W. , and Jones, M.C. , Paper presented at Cryog. Eng. Conf., Boulder 1977
47. Campbell, M.E. , Loser, J.B., and Sneegas, E., Solid Lubricants, NASA SP-5059, May 1966
48. Stekly, Z.J.J., J. Appl . Phys. , Vol. 42, p. 65, 1971
49. White, G.K., "Experimental Techniques in Low-Temperature Physics", Clarendon Press, Oxford, 1959
50. Brechna, H., "Superconducting Magnet Systems", Springer, New York, 1973

1. Report No. <b>NASA CR-2963</b>		2. Government Accession No.		3. Recipient's Catalog No.	
4. Title and Subtitle <b>CRYOGENIC-COOLANT He<sup>4</sup>-SUPERCONDUCTOR INTERACTION</b>				5. Report Date <b>April 1978</b>	
				6. Performing Organization Code	
7. Author(s) <b>S. Caspi, J. Y. Lee, Y. I. Kim, R. J. Allen, and T. H. K. Frederking</b>				8. Performing Organization Report No. <b>UCLA-ENG-7767</b>	
				10. Work Unit No.	
9. Performing Organization Name and Address <b>University of California at Los Angeles School of Engineering and Applied Science Los Angeles, California 90024</b>				11. Contract or Grant No. <b>NSG-3153</b>	
				13. Type of Report and Period Covered <b>Contractor Report</b>	
12. Sponsoring Agency Name and Address <b>National Aeronautics and Space Administration Washington, D.C. 20546</b>				14. Sponsoring Agency Code	
15. Supplementary Notes <b>Final report. Project Manager, James Burkhart, Physical Science Division, NASA Lewis Research Center, Cleveland, Ohio 44135.</b>					
16. Abstract <p>The thermodynamic and thermal interaction between a type II (NbTi-Cu)-composite alloy and cryo-coolant He<sup>4</sup> has been studied with emphasis on post-quench phenomena of formvar-coated conductors. The latter have been investigated using a heater simulation technique. Overall heat transfer coefficients were evaluated for the quench onset point. In addition, heat flux densities were determined for phenomena of thermal switching between a peak and a recovery value. The study covered near-saturated liquid, pressurized He<sup>4</sup>, both above and below the lambda transition, and above and below the thermodynamic critical pressure. In addition, friction coefficients for relative motion between formvar-insulated conductors were determined.</p>					
17. Key Words (Suggested by Author(s)) <b>Post-quench scenario of superconducting composite conductors; Low temperature coolant He<sup>4</sup>; Super-critical fluid; Lambda transition; Heater simulation technique; Thermal conductances; Quench onset; Friction coefficients</b>				18. Distribution Statement <b>Unclassified - unlimited STAR Category 34</b>	
19. Security Classif. (of this report) <b>Unclassified</b>		20. Security Classif. (of this page) <b>Unclassified</b>		21. No. of Pages <b>91</b>	
				22. Price* <b>A05</b>	



**END**

**9.21.78**